Development of Ionic Polymer Metallic Composites as Sensors

By

David J. Griffiths

Thesis submitted to the Faculty of Virginia Polytechnic Institute and State University

in partial fulfillment of the requirements for the degree of

Master of Science

in

Mechanical Engineering

Pavlos P. Vlachos, PhD, Co-Chair

Donald J. Leo, PhD, Co-Chair

Michael Roan, PhD, Committee Member

September 26, 2008

Blacksburg, Virginia

Keywords: Ionic Polymer Metallic Composite, Sensor, Bio-Acoustics

 Contact: dagriff2@vt.edu

TABLE OF CONTENTS

List of Figures iii

List of Tables v

Abstract vi

Chapter 1 Introduction and Background 1

Introduction 1

1.1 History 1

1.2 Overview of IPMCs 2

1.2.1 Review of the current modeling for IPMC sensors 4

1.2.2 Review of characterization efforts on IPMC sensors 11

1.2.3 Review of current applications of IPMC sensors 15

1.3 Proposed Contribution 19

Chapter 2 Characterization 20

Introduction 20

2.1 Experimental Setup 20

2.1.1 Impedance Spectroscopy 25

2.1.2 Scanning Electron Microscopy 31

2.1.3 Bending Sensitivity 34

2.2 Results 42

2.3 Conclusion 46

Chapter 3 Development of a Bio-Acoustic sensor 48

Introduction 48

3.1 Design of a bio-acoustic sensor 50

3.2 Testing and validation of the bio-acoustic sensor 52

3.3 Conclusion 56

Chapter 4 Concluding remarks and future recommendations 58

Acknowledgments 62

Bibliography 63

LIST OF FIGURES

Figure 1.1 Histogram of IPMC sensor publications 2

Figure 1.2 Breakdown of emphasis on topics 2

Figure 1.3 Dissection of an IPMC 2

Figure 1.4 Histogram of the published sensing models 5

Figure 1.5 History of characterization papers 12

Figure 1.6 Progression of IPMCs into physical sensors 15

Figure 2.1 Schematic of the signal conditioner 22

Figure 2.2 Signal to noise ratio at 10 Hz and broadband rms 23

Figure 2.3 Autolab potentiostat/galvanostat 25

Figure 2.4 Bode plot of impedance data for group 1 26

Figure 2.5 Bode plot of impedance data for group 2 26

Figure 2.6 Bode plot of impedance data for group 3 26

Figure 2.7 Bode plot of impedance data for group 4 26

Figure 2.8 Bode plot of impedance data for group 5 26

Figure 2.9 Nyquist for group 1 27

Figure 2.10 Nyquist for group 2 27

Figure 2.11 Nyquist for group 3 27

Figure 2.12 Nyquist for group 4 27

Figure 2.13 Nyquist for group 5 27

Figure 2.14 Capacitance and resistance for sensors in group 1 28

Figure 2.15 Capacitance and resistance for sensors in group 2 28

Figure 2.16 Capacitance and resistance for sensors in group 3 28

Figure 2.17 Capacitance and resistance for sensors in group 4 29

Figure 2.18 Capacitance and resistance for sensors in group 5 29

Figure 2.19 Ideal Randle circuit 29

Figure 2.20 Calculated values on the charge transport resistance 30

Figure 2.21 Calculated ionic conductivity values for all sensors....31
Figure 2.22 Calculated normalized capacitance values for all sensors....31
Figure 2.23 Typical image generated from the ESEM....32
Figure 2.24 Comparison of the electrode architecture....33
Figure 2.25 Comparison of the ionomer thickness....34
Figure 2.26 Deviation of the mean between the five sets....34
Figure 2.27 Bending test setup for a sensitivity comparison....35
Figure 2.28 Sensitivity at 30 Hz with respect to tip displacement of the transducer....38
Figure 2.29 Sensitivity at 30 Hz with respect to strain energy....38
Figure 2.30 Calculated transfer function and coherence for a single sample with varying amplitudes....40
Figure 2.31 Transfer function and coherence of the discrete method....41
Figure 2.32 The discrete transfer function overlaid with white noise input method....41
Figure 2.33 Relation between the electric double layer capacitance and sensitivity....43
Figure 2.34 Relation between ionic conductivity resistance and sensitivity....43
Figure 2.35 Relation between charge transport resistance and sensitivity....43
Figure 2.36 EDL capacitance and electrode thickness....44
Figure 2.37 EDL capacitance and volume of conducting powder....44
Figure 2.38 Ionic conductivity and electrode thickness....45
Figure 2.39 Ionic conductivity and ionomer thickness....45
Figure 2.40 Charge transport resistance to electrode thickness....45
Figure 2.41 Charge transport resistance to ionomer thickness....45
Figure 2.42 Sensitivity per unit work compared to ionic conductivity....46
Figure 2.43 Sensitivity per unit work compared to ionomer thickness....46
Figure 3.1 Cross section of the cantilevered configuration, and actual picture with the wiring exposed....50
Figure 3.2 Sensitivity per unit radian....51
Figure 3.3 Predicted center displacement for a reference pressure of 1 Pa....52
Figure 3.4 Unfiltered time series of the pressure waveform....53

Figure 3.5 Three cycles distinguishing the systolic and diastolic phase 53

Figure 3.6 Comparison of the power spectral density's over the entire bandwidth 54

Figure 3.7 Comparison of signal power in the in the low to infrasonic bands 54

Figure 3.8 Difference in gain in the magnitude of the voltage within their frequency band 55

Figure 3.9 Left. Spectrogram from the IPT based stethoscope over the compete bandwidth. Right. Spectrogram from the 3M. Both showing 4 cycles 56

Figure 3.10 Left. Spectrogram from the IPT based stethoscope for infrasonic. Right. Infrasonic and low frequency shown from the 3M 56

Figure 4.1 Sensitivity compared to the measured electric double layer capacitance 58

Figure 4.2 Electric double layer capacitance compared to expected RuO_2 volume 58

Figure 4.3 Comparison of mechanical work to electrical current for transducers of similar sensitivity and varying charge storage capacity 59

Figure 4.4 Ionic conductivity compared to ionomer thickness 59

Figure 4.5 Sensitivity compared to interfacial resistance 60

Figure 4.6 Bending sensitivity of a 2 mm cantilevered IPT 60

Figure 4.7 Acquired arterial pressure waveform 61

Figure 4.8 Acquired cardiac sounds 61

LIST OF TABLES

Table 2.1 21

Table 2.2 24

ABSTRACT: DEVELOPMENT OF IONIC POLYMER METALIC COMPOSITES AS SENSORS

By: David Griffiths

Ionomeric polymer transducers (IPTs) are an exciting new class of smart materials that can serve a dual purpose in engineering or biomedical applications as sensors or actuators. Most commonly they are used for mechanical actuation, as they have the ability to generate large bending strains and moderate stress under low applied voltages. Although the actuation capabilities of IPTs have been extensively studied, the sensing capabilities of these transducers have yet to be fully explored. The work presented herein aims to investigate the fundamental sensing characteristics of these transducers and apply the acquired knowledge toward the development of an electronic stethoscope for digital auscultation. The sensors were characterized both geometrically and electrically to determine their effectiveness in resolving a signal from sub 1 Hz to 2 kHz. Impedance spectroscopy was used to interrogate the sensing mechanism. Following the characterization of the transducer, a bio-acoustic sensor was designed and fabricated. The bio-acoustic sensor was placed over the carotid artery to resolve the arterial pressure waveform in situ and on the thorax to measure the S1 and S2 sounds generated by the heart. The temporal response and spectral content was compared with previously known data and a commercially available electronic stethoscope to prove the acquisition of cardiovascular sounds.

CHAPTER 1 INTRODUCTION AND BACKGROUND

INTRODUCTION

This section contains a historic overview of Ionic Polymer Metallic Composites (IPMCs). The first section will review the history of the development of the material. Included in this section will be a comprehensive review of the progress of IPMCs as sensors. The proceeding sections are divided into three main categories; a review of the modeling of IPMCs as sensors, a review of the current work to characterize IPMCs as sensors, and a review of devices that have been developed using IPMCs.

1.1 HISTORY

In the late 1940's and early 1950's the ability of ionic polymers to be used as electromechanical actuators was first discovered [1, 2]. The work was sparsely continued from the 1960's to the mid 1980's [3-6], leaving active ionic polymers relatively underdeveloped and underutilized. In 1992, a revitalization of this technology was brought about by Oguro [7] and Shahinpoor [8] for actuation and Sadeghipour [9] for sensing. Since that time Ionic Polymer Metallic Composites (IPMCs) have attracted considerable attention as actuators due to their ability to produce large strains and moderate stress under small applied potentials. From 1992 through 1997 an estimated 400 publications [10] pertaining to IPMCs had been published, of which approximately 31 were directly related to sensing, with more emerging in 2008. Figure 1.1 is a histogram of the progression of IPMCs as sensors from 1992 to 2007. Figure 1.1 indicates an increase in interest toward IPMCs as sensors as the technology matures, with 2005-2007 accounting for 44% of all publications. Figure 1.2 represents the distribution of research into three fundamental topics; modeling the transduction mechanism, characterization of material

parameters toward sensing performance, and application of IPMCs as sensors. Currently the research efforts have had an emphasis on modeling the transduction mechanism however characterization has received less attention.

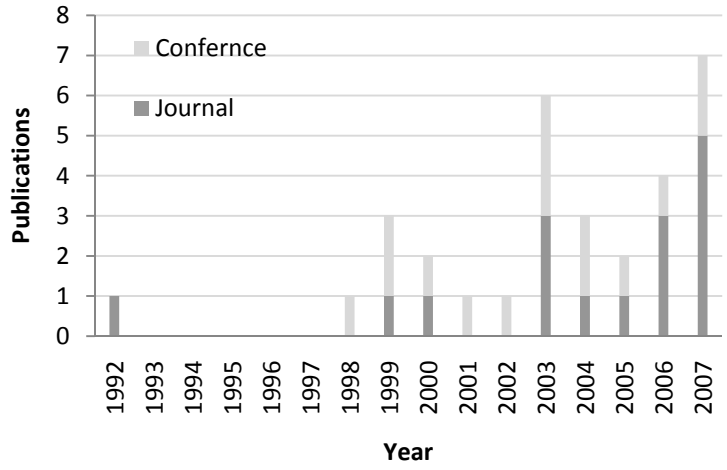

Figure 1.1 Histogram of IPMC sensor publications

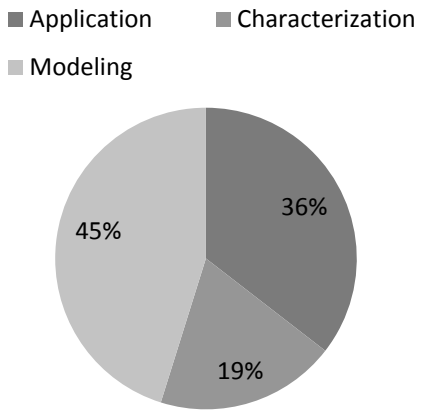

Figure 1.2 Breakdown of emphasis on topics

1.2 OVERVIEW OF IPMCS

Ion select polymers are a type of material that exhibits ionic selectivity and ionic mobility. Ionic polymer metallic composites are composite materials consisting of a perfloronated ionic polymer typically DuPont's Nafion or Asahi Glass's Flemion. The ionomer is sandwiched between two high surface area interfacial electrodes that have a high conductivity surface layer attached, seen in Figure 1.3.

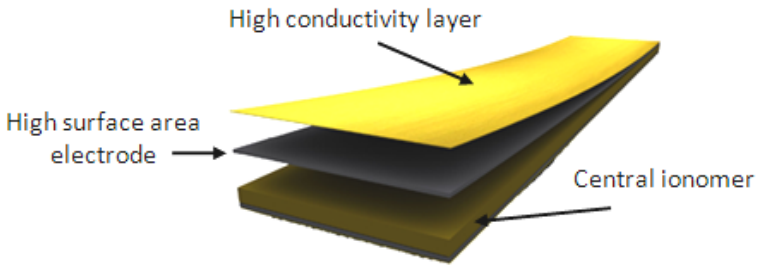

Figure 1.3 Dissection of an IPMC

It is generally believed that an electrical potential difference across the ion exchange membrane initiates a migration of the cations and the electrostaticly clung diluent toward the anode. The mass transport phenomena of hydrated cations create a pressure gradient through the thickness of the transducer, causing the structure to deform [11, 12]. It is also believed that these materials exhibit reciprocity, in that under a mechanical deformation the mobile cations will propagate in response to a stress gradient and can be measured as a current, potential, or charge [13-15].

The three most common methods to fabricate an ionic polymer metallic composite consist of the impregnation reduction process, physical casting techniques, and the Direct Assembly Process (DAP). The first method, impregnation reduction, which was originally investigated for purposes other than IPMC fabrication [16, 17] utilizes the ionic selectivity of the ion exchange membranes. First the membrane is allowed to soak in a metal salt solution, typically $PtNH_3Cl_2$. Then the membrane is soaked in a reducing agent, leaving metallic dendritic formations penetrating into the ion exchange membrane. The effectiveness of this method continues to make it the most popular fabrication technique. However, the impregnation reduction process is slow, expensive, and allows for little control over the conducting electrodes geometry. Electrode geometry has been linked to actuation performance of the transducer [18-23] making this an important parameter to regulate during fabrication. Multiple studies have been performed using the impregnation reduction method, but the variability from sample to sample created from this method makes it difficult to draw definitive conclusions and repeatable results that may be readily reproduced. Another effort to try to control the architecture better than the chemical reduction process is a physical assembly of

the varying layers of the composite through casting [24-26]. Casting allows for direct control over the diluent loading and geometry of the transducer, however, this method is also plagued by inconsistency between samples. In order to achieve greater consistency and repeatability while maintaining control of the electrode architecture and microstructure the Direct Assembly Process was developed [27]. The DAP has two variations; one where an electrode is applied to a dry membrane and another where the electrode is applied to a solvated membrane. This method physically assembles the electrode by creating a mixture of conducting particles, ionic liquid, unmodified 5% Nafion dispersion and isopropanol as a solvent that will readily evaporate. The physical deposition of the electrode solution is done by either painting, spraying or printing [28].

1.2.1 REVIEW OF THE CURRENT MODELING FOR IPMC SENSORS

Through the development of ionic polymer metallic composites as sensors there have been multiple attempts to model the transduction method. Most of these models stemmed from actuation but are electromechanically coupled, allowing for the sensing response given a mechanical input. The papers will be discussed in chronological order. Most authors took one of three approaches, a black box model, a gray box model, or a white box model. A black box model dictates that there is no prior knowledge of the system, a gray box model indicates some system knowledge, and a white box model is based on a purely physical derivation. Figure 1.4 illustrates the chronological progression of published sensing models from 1992 through 2007.

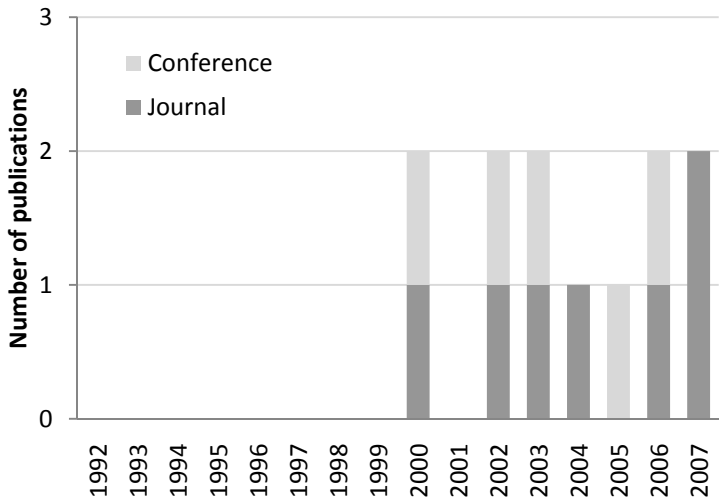

Figure 1.4 Histogram of the published sensing models

The first effort to model the electromechanical response from an IPMC mathematically was done by Nemat-Nasser in 2000 [29, 30]. Nemat-Nasser presented a white box model to describe the transduction mechanism based on ion transport, elastic deformation and an electric field. The author indicated that a sudden change in the IPMC's shape would induce a stress on the backbone of the polymer. To compensate an electric potential would be generated which would cause a relocation of the effective centers of the fixed anions and mobile cations within a cluster, forming a dipole. The author continued to find how much the effective charge centers displace assuming a spherical cluster, and ultimately found the potential generated by the separation distance. This led to an expression for the electric field generated in the polymer at some given point induced by the dipole. The electric field, E, was calculated by finding an average value for the electric field on the boundary of two clusters and summed yielding:

$$E = 2\sum_{n=0}^{n=\infty} \frac{1}{(2n+1)^3} \frac{1}{4\pi\kappa_w} \frac{3}{\frac{2\kappa_p}{\kappa_w}+1} \frac{2\mu}{(r_d/2)^3}$$

and the potential difference, ΔΦ, across the thickness was given as:

$$\Delta\phi = 2hE$$

where k_w is the dielectric constant of the diluents, k_p is the dielectric constant for the polymer, μ is separation of the charge centers, and r_d is the effective cluster radius. The author observed good experimental agreement with the analytical solution, and made a note that the voltage generated by a deformation was two orders of magnitude less than what was required to generate the same deformation. Newbury developed a gray box model in 2002 which was a linear two port model that can go between sensing and actuation based on a coupled electromechanical response [14, 31]. This model was later improved in 2003 to include viscoelastic effects and geometric scalability [12]. The model was formed by constructing an equivalent circuit with the mechanical and electrical transformation being modeled by a linear transformer with N number of turns. The relation took the form:

$$\begin{Bmatrix} v(\omega) \\ f(\omega) \end{Bmatrix} = \begin{bmatrix} Z_{11} & Z_{12} \\ Z_{21} & Z_{22} \end{bmatrix} \begin{Bmatrix} i(\omega) \\ \dot{u}(\omega) \end{Bmatrix}$$

where v is voltage, f is force, *i* is current and $\dot{u}$ is velocity. The values for Z_{11} through Z_{22} were derived from the mechanical and electrical impedances. There were two mechanical impedance terms, one was mechanical stiffness derived from Euler-Bernoulli, and another was an inertial term with the inclusion of viscoelastic effects developed by McTavish and Hughes. There were two electrical impedance terms in the model, the first being a DC resistance and the

second representing the transducers charge capacity. Newbury continued to solve the system of equations using voltage and current relationships and a mesh current to find the actuation and sensing characteristic equations. Newbury showed that an input output relation could easily be derived. Two examples derived by Newbury were a current output for a given tip velocity:

$$\left(\frac{i}{\dot{u}}\right) = \frac{-3dtwY^E}{4L_d}$$

and a voltage for a given force, assuming operation below the first resonance:

$$\left(\frac{v}{f}\right) = \frac{3d{L_d}^2}{\eta^T L_t wt}$$

given that d is the piezoelectric coupling, t is the thickness, w is the width, Y^E is the frequency dependent Young's Modulus, L_d is the distance along the IPMC where the perturbation occurs, and η^T is the frequency dependent number of turns for the transformer. The interested reader should refer to [12, 32]. Also in 2003 Farinholt published his results on modeling the charge sensing capabilities of ionic polymers [13], which he followed up in 2004 [33]. Farinholt developed an expression relating electric field, charge density and electric potential under short circuit conditions from electrostatic field equations. Farinholt hypothesized that the charge density on the surface of the polymer is proportional to stress. Using the field equations introduced by Nemat-Nasser, Farinholt derived a PDE that modeled the spatial and temporal distribution of charge from a disturbance:

$$\frac{\partial \rho}{\partial t} - d\nabla^2\rho + \frac{\mathrm{F}^2\mathrm{dC}^-}{\kappa_c \mathrm{RT}}(1 - \mathrm{C}^-\Delta\mathrm{V})\rho = 0$$

where ρ is the charge density, t is time, d is the diffusion coefficient, F is Faraday's constant, C^- is the anion concentration, κ_c is the dielectric permittivity, R is the gas constant, T is the absolute temperature and ΔV is volumetric change. The PDE was solved using separation of variables to find the charge density, ρ, as a function of time and space:

$$\rho(x,t) = \frac{\rho_0}{\sinh(\beta h)} \sinh(\beta x)\, e^{-\lambda t}$$

where ρ_0 is the initial charge density, x is the position in the transducer, β is the reciprocal of length and is defined as $\sqrt{\frac{\tau-\lambda}{d}}$, and λ is an inverse time constant. To calculate the potential the charge density must be integrated. After application of the boundary conditions the potential in space and time can be solved. Interestingly, this showed the charge density is virtually zero everywhere except toward the surface of the polymer. Farinholt continued to find what the charge and current would be under an imposed deformation, w, at some position, L, as:

$$q(t) = w(L)\frac{Y}{\beta\psi_s}\frac{3}{2}\frac{bh}{L}e^{-\lambda t}$$

$$i(t) = -\lambda w(L)\frac{Y}{\beta\psi_s}\frac{3}{2}\frac{bh}{L}e^{-\lambda t}$$

with b representing the sample width, h the distance from the neutral axis, L the length of the polymer, and Ψ_s as the stress charge proportionality constant. Farinholt had good agreement with the experimental data, however, there was a phase-lag that was attributed to the capacitance of the signal conditioning circuit. Buechler in 2005 used the idea of

electromechanical coupling and adopted an energy based approach to model an IPMC [34]. Buechler later revised his work and published it in 2007 [35]. Using Hamilton's principle he stated the difference in the variation of the kinetic and potential energy summed over a time interval plus the variation of external work must equate to zero. Buechler continued through his derivation and arrived at two coupled differential equations, with frequency dependent parameters such as the elastic modulus, strain coefficient, and dielectric permittivity. The final relation was found to be:

$$\begin{Bmatrix} \underline{A}(j\omega) \\ \underline{q}(j\omega) \end{Bmatrix} = \begin{bmatrix} -\boldsymbol{M_s}\omega^2 + \boldsymbol{K_s}(j\omega) & \underline{\psi}(j\omega) \\ \underline{\psi'}(j\omega) & C^{-1}(j\omega) \end{bmatrix}^{-1} \begin{Bmatrix} \underline{\Phi_u'}\mathrm{f}'(\mathrm{j}\omega) \\ \underline{V'}(j\omega) \end{Bmatrix}$$

where M_s is the mass matrix, K_s is the stiffness matrix, Ψ is the coupling vector, and C is the capacitance. This equation can be reduced to show either the actuation output under an applied potential, voltage or charge output from an input force. One example for the transfer function between voltage and force was given as:

$$\frac{V(j\omega)}{f(j\omega)} = \psi'[-\boldsymbol{M_s}\omega^2 + \boldsymbol{K_s}(j\omega)]^{-1}\underline{\Phi_u}'$$

where V is voltage and f is forcing. There were three papers published in 2006. Pudipeddi presented a model for sensing that was previously developed by Konyo [36]. Pudipeddi formulated the voltage output using an equivalent circuit model based on the assumption that a production of charge accumulates on the surface of an IPMC under a mechanical deformation [37]. Pudipeddi used an equation of motion for a long slender beam with an added viscous

dampening term. This combined with the equivalent circuit yielded the voltage, V, expressed as:

$$V = \frac{\alpha \int_l \; v(x,t)dt}{\frac{R_i C_l}{2R_i + R_{ei}}\left[1 - e^{-\left(\frac{2R_i + R_{ei}}{R_i C_l R_{ei}}\right)}\right]}$$

This model predicted an increase in voltage and displacement for a longer length beam, and decreased voltage amplitude subject to higher frequency excitation. The author's model exhibited good agreement with the experimental data. The author continued to test three separate samples with three different cation species. He concluded there was no discernable difference between the samples. In 2006 Bonomo proposed an alteration to Newbury's model [38]. The author found the sensors also have a dependency on hydration, but work better when they are in equilibrium with the environmental humidity and not fully saturated. Bonomo found new values for d and Y that pertain to an environmentally hydrated sample. There was good agreement between the model and the experimental data from 1-200 Hz with varying length transducers. The final paper to introduce a model was presented in 2007 by Chen. Chen created a dynamic model for IPMC sensors [15] based on the foundations set by Nemat-Nasser and Farinholt with the addition of surface resistance. Chen analytically solved the PDE's in the Laplace domain allowing for the analysis of an arbitrary input. Chen found the sensor output, i(s), with respect to the displacement, w(s), using:

$$\frac{i(s)}{w(s)} = \frac{3sYW(\beta(s)hcoth(\beta(s)h) - 1)}{\alpha_0 L^3 \beta^2(s)} \frac{1 - \cosh\left(\sqrt{B(s)}L\right) + \sqrt{B(s)}Lsinh(\sqrt{B(s)}L))}{B(s)\cosh\left(\sqrt{B(s)}L\right)}$$

with $(s) = \sqrt{\frac{s+K}{d}}$ and $B(s) = \frac{s\kappa_c r_0}{h}$, Y is the Young's modulus, W is the width of the beam, h is the distance from the neutral axis to the surface, L is the free length and α_0 is the charge stress coupling constant. The author continued the derivation to produce a lower order model that can be implemented with a design. Chen continued to verify the model and saw a slightly closer agreement with the experimental data compared to Farinholt's derivation, when the surface resistance was taken into account. The response of the transducer was characterized up to 20 Hz in Chen's experiment.

1.2.2 REVIEW OF CHARACTERIZATION EFFORTS ON IPMC SENSORS

A thorough characterization of IPMCs is paramount to understand the fundamental mechanism of transduction. Figure 1.5 shows the progression of papers that have been written to solely characterize the properties of an IPMC, such as the cation species, and their effect on sensing. Material properties have been investigated for model validation and are covered in the modeling section. What can be concluded is an increase in characterization efforts as the technology grows, but the current knowledge base is limited to only a few studies.

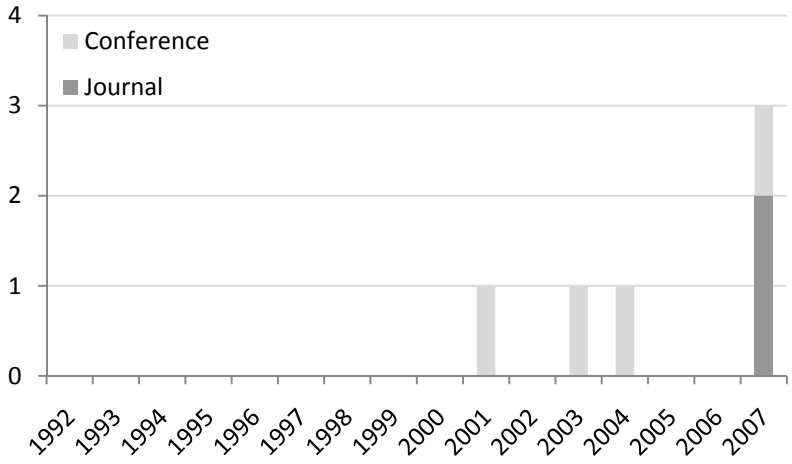

Figure 1.5 History of characterization papers

In this section the current results will be presented from the papers that solely demonstrate a characterization of alterable parameters. There have been approximately six papers published that go into depth to characterize the alterable parameters such as the diluents viscosity, dielectric permittivity, the cation species, and electrode properties. The first paper, published in 2001 by Shahinpoor, reviewed the electrical properties and response of IPMC sensors [39]. Shahinpoor followed the example set by de Gennes [40] who stated the sensing phenomena is based on irreversible thermodynamics. The two major contributors are an ion transport and an electrophoretic solvent transport. The electric field generated from an imposed torque was found using:

$$\vec{E} = \frac{12(1-\sigma_p)}{1-2\sigma_p}\frac{L}{\sigma h^3}\Gamma$$

where σ_p is the Poisson ratio, h is the strip thickness, and Γ is the imposed torque. Shahinpoor stated the output can be found with knowledge of the Poisson ratio and conductance. Impedance tests were performed on various samples fabricated using the impregnation

reduction method. The impedance tests indicated changing the depth of penetration of the platinum could alter the conductance. In general the deeper the platinum imbeds into the surface, the lower the conductance. In 2003 Bonomo presented a characterization of the frequency response of an IPMC. In this preliminary document, it was observed that a nonlinearity tends to emerge at lower frequency excitations and a larger phase offset. The tests preformed ranged from 3.69 to 5.60 Hz. Another observation was consistent amplitude across the range of frequencies tested. In 2005 Bonomo published a method to characterize the deformation of an IPMC [41]. A measurement device was constructed using an actuated IPT placed in between two metal plates. The device was characterized and used to measure the displacement of an IPMC by monitoring the change in capacitance between two parallel plates in which the IPMC was oscillating. From the initial tests to characterize an IPMC the author concluded the output from the transducer tended to have a derivative effect. In 2004 Farinholt published preliminary findings to a counter ion, diluent, and loading study and their effects on sensitivity [42]. In 2007 he published the conclusion to the work which is the first journal article to address characterization for an IPMC sensor [43]. Farinholt stated ionic polymer transducers (IPTs) can be tailored as a function of polymer structure, fixed and mobile ionic groups, diluent properties and surface electrode treatments. There are three modes in which an IPMC can be used as a sensor; bending, stretching, and compression. He concluded that both bending and applied pressure have similar sensitivities, where as in elongation the sensitivity is 1-1.5 orders of magnitude lower. He also observed electrical impedance and sensitivity changes if the material was prestrained. He continued to compare the sensing response to varying cation species. He tested three monovalent cations, Li^+, Na^+, Cs^+, one divalent cation, Ca^{2+}, and two

large organic cations, tetraehtylammonium (TEA^+) and tetrabutylammonium (TBA^+). Farinholt concluded Li^+ and Cs^+ provided the highest sensing response, and alkali cations tended to experience a reduction in the low frequency response. In general larger cations led to a larger electrical resistance and a lower sensitivity. Through normalizing the sensors output by its impedance, Fairnholt observed that the sensing characteristics tended to merge, which indicated the electrical impedance played a direct role in the performance of the transducer. Next, Farinholt altered the diluents by mixing glycerol with water in various percentages. He found the electrical resistance tended to increase with an increase in viscosity and a decrease in dielectric permittivity. The increase in electrical resistance can be thought of in a physical analogy to an increase in resistance to diffusion. The increase in resistance due to the viscosity and decrease in dielectric permittivity were found to both slow the frequency response and have a detrimental effect on the sensitivity. One other phenomenon was observed when butyl acetate was used as the diluent. Butyl acetate has a dielectric permittivity about 15 times lower than water. An anti-resonance was observed around 1 Hz indicating there is a secondary mechanism contributing to both the sensing and actuation mechanism. In 2007 Griffiths correlated electrical properties to the physical dimensions of the electrode and sensitivity when IPMCs were used for a wall shear stress sensor [23]. This work supported the findings by Fairnholt. Thicker electrodes were found to have a higher capacitance and greater sensitivity. It was also found that the physical geometry of the ionomer did not play a substantial role for the transducer's sensitivity, and acted as a passive layer. The final paper published in 2007 was by Punning and demonstrated how the surface resistance changed as the IPMC deforms [44]. Punning showed the deformation of a transducer changes the surface resistance of the tensile

side and minimally on the compressive side. A delay associated with the output signal was observed if the resistance in the surface electrode was increased. The amplitude and reproduction of the signal severely deteriorated with an imbalance in the surface resistance. In 2008 Takagi published findings on the frequency response characteristics of IPMCs [45]. The author found that Na^+ has a higher sensitivity than TBA in current and charge sensing modes, yet interestingly slightly lower sensitivity in a voltage sensing mode.

1.2.3 REVIEW OF CURRENT APPLICATIONS OF IPMC SENSORS

The development of IPMCs into functional sensors has been relativity slow and sporadic. Figure 1.6 shows the progression of IPMCs as physical sensors from 1992-1997.

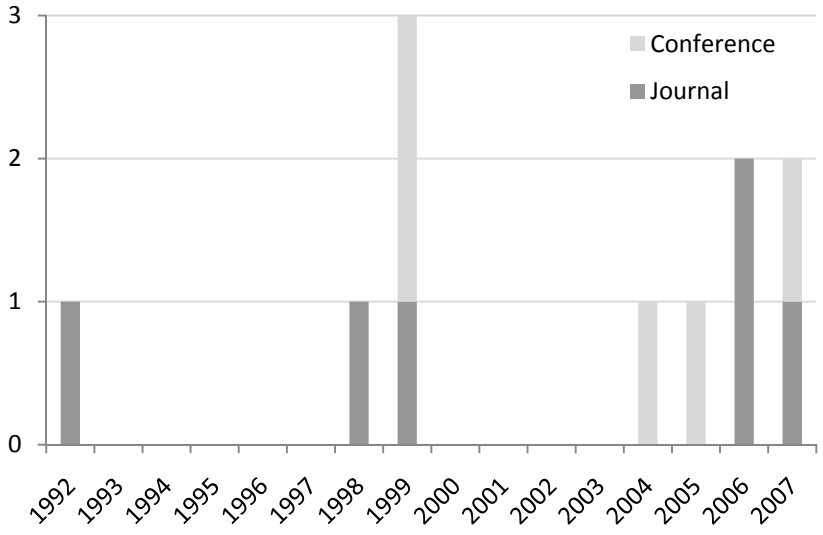

Figure 1.6 Progression of IPMCs into physical sensors

The first use of an IPMC as a sensor was developed by Sadeghipour [9]. Sadeghipour developed a cell that consists of an ionomer plated with platinum electrodes. The cell had chambers on either side of the IPMC that were evacuated of air and filled with hydrogen gas. The pressure difference triggered a proton migration, and created a potential difference across

the thickness of the ionomer. The cell produced an open circuit voltage that is governed by the Nerst equation:

$$E = \frac{RT}{2F} ln\left(\frac{P_1}{P_2}\right)$$

where R is the gas constant, T is the absolute temperature, F is the Faraday constant and P_1 and P_2 are the pressures in each cell. Sadeghipur showed this concept could be used to develop an accelerometer that had a bandwidth up to 2000 Hz. In 1998 Shahinpoor [46] presented a general review where he showed an IPMC in a clamped cantilevered beam configuration can be used as a motion sensor. His findings indicated that there is a linear relationship between the voltage output and an imposed quasi-static displacement. In 1999 Ferrara developed a concept to use an IPMC as a pressure transducer in the human spine [47]. Ferrara observed IPMCs are biologically neutral and fluid has a tendency to enhance the performance by maintaining a consistent working environment. Ferrara developed an experimental setup where an IPMC was given a compressive load by a uniaxial materials testing system and measured the response from the IPT. Ferrara reported a non-linear output was observed and argued it was caused by the viscoelastic nature of Nafion. Also in 1999 Keshavarzi introduced a concept to use IPMCs as a blood pressure, pulse rate, and rhythm measurement device [48]. Keshavarzi developed an experiment to press on an IPMC with a nylon screw, exerting a load from 5 grams to 55 grams on a transducer that is 0.5 by 0.5 cm^2 which translates to a pressure range of 15-165 mmHg. Keshavarzi reported a linear voltage output with respect to magnitude in the range that was measured with a slightly asymptotic behavior at the higher loads. Unfortunately this study did not include any actual data correlating with current medical devices to show it can work, only that there is a possible potential for such a device to work. The next paper published was in

2004 where Konyo developed a velocity sensor [36] using IPMCs. Konyo used the premise brought forth by Yamagami-Tadokoro [49] where two hypotheses on the sensing mechanism were formed; cation migration caused by swelling and contraction of the ionomer, and cation migration caused by inertial forces. Konyo stated that either or both are responsible for the polarization of electrical charge. This paper showed how the voltage output from a transducer can be related to the velocity. Konyo found a relationship of approximately 10 mV/m/s. The simulation based on the assumed transduction mechanism agreed well with the experimental results. After the derivation, a sensory ball was developed with an IPMC sensor imbedded in a PDMS housing in a cross formation. When the ball was manipulated the response from the imbedded IPMC was used to find the direction and velocity of the ball. Konyo was able to accomplish this, successfully supporting the claim of a velocity driven sensor. In 2005 Etebari introduced the use of an IPMC for wall shear stress measurements [50]. In this paper Etebari encapsulated an IPMC between Mylar and Kapton using an ionic liquid as the diluent. Etebari showed the sensors potential of picking up separation but stated that any DC shear measurement was not possible due to the capacitive nature of the transducer. There were two journal papers published in 2006, one by Biddiss and one by Bonomo. Biddiss hoped to use IPMCs as a compliant sensor in a hand prosthesis [51]. Biddiss found there was a linear relationship to the curvature of the IPMC and the output voltage as long as the bending rate is greater that 0.75^{o} min^{-1}. Biddiss also concluded the IPMC could not be used for a DC measurement, so a controls device would have to be designed to buffer the current position and find the new displacement based on the sensor output. Bonomo used an IPMC as a force sensor by forcing it to resonate. From Euler-Bernoulli beam theory the mechanical resonance

will change as an axial load is altered. Bonomo forced the IPMC to a resonance by exciting it with an AC source and monitoring the displacement of the IPMC with infrared transmitters and receivers. The axial force can be back calculated from Euler-Bernoulli knowing the material properties and the resonant frequency. This is the only IPMC based system to date that can measure DC, but it requires the use of a different transducer to sense the mechanical input. In 2007 there were two more papers published, one by Punning and another by Wang. Punning took a unique approach to develop a self-sensing IPMC actuator [52]. Punning previously reported that the electrode resistance changes on the tensile side, and remains fairly constant on the compressive side when bent. This concept was used to correlate bending curvature to surface resistance on the electrodes. Measurement of the surface resistance allowed for accurate control of the IPMC while actuating. Wang developed a tactile sensor based on IPMCs [53]. Wang used the idea brought forth by Newbury that an induced stress will trigger a capacitive discharge that is measurable. Wang encapsulated an IPMC strip based on Nafion and Flemion in a PDMS ball. Wang observed a voltage output when the tactile sensor was pressed and related it to force. Wang observed that the sensing signal decays in time with Nafion based transducers, but not a Flemion based transducer. The most recent application of IPMC sensors has been presented by Andò in March of 2008. Andò created a toroidal device that can be used to detect equilibrium variations [54]. The author used a combination of IPMCs and ferrofluid to determine orientation. The concept was contrived from the vestibular system in the inner ear that humans use for balance.

1.3 PROPOSED CONTRIBUTION

From the review it is apparent there has been little effort in the community to fully characterize an ionic polymer metallic composite for sensing when compared to actuation. This document will present a detailed study of the electrodes and the ionomer, their architecture, electrical properties and the effect they have on sensing. Using this information a dynamic pressure transducer will be developed, demonstrated and compared to a commercial device. The author aspires to show:

- The sensitivity of an ionic polymer transducer is directly proportional to the charge storing ability of the electrode
- The charge storage mechanism of the high surface area electrode is based on the electric double layer capacitance
- Reducing the ionic conductivity resistance will increase the energy conversion from mechanical work to an electrical current for a given transducer
- The sensitivity range of the transducers extends well beyond the previously reported 500 Hz, and it is documented herein as high as 2000 Hz
- An ionic polymer metallic composite can be used as a bio-acoustic sensor, and demonstrate its capabilities through in situ testing

CHAPTER 2 CHARACTERIZATION

INTRODUCTION

In the previous section a review of ionic polymer metallic composites as sensors was presented, and demonstrated a full characterization of IPMC sensors has yet to be completed. Akle has previously shown how the electrode architecture is directly related to the through thickness impedance, and the maximum strain obtainable for an actuator [18, 19]. It is believed the central ionomer acts as a passive layer and the electrode is the active layer of the composite. In this section similar experiments are conducted to show a reciprocal behavior for sensing. Experimental evidence will be presented to support this notion and help enhance the understanding of the transduction mechanism.

2.1 EXPERIMENTAL SETUP

In this section the fabrication procedures are presented first, followed by the signal conditioner characterization, the bending sensitivity tests, and electrical impedance measurements. Data is presented to quantify the geometric parameters found through scanning electron microscopy.

FABRICATION OF SAMPLES

Akle developed a novel fabrication process for ionic polymer transducers entitled the Direct Application Process (DAP) [55]. The DAP allows the use of any type of ionomer, diluent, and conducting powder to form the transducer. With the added control over fabrication the electrode architecture and composition of the transducer can be tailored for a wide range of applications. The first step in the DAP is to perform a cation exchange. The monovalent Li^+ was chosen since it was used as a baseline for Fairhholt's cation characterization. Next Nafion was

dried then swollen with 1-ethyl-3-methyimidazolium trifluoromethanesulfonate (EmI-Tf) by heating. Bennett and Leo [56] demonstrated EmI-Tf is an air stable diluent with acceptable performance for actuation. After the solvent was imbibed into the membrane, the electrodes were applied using an air-brush. The electrode dispersion fluid was prepared containing a mixture of the 5% Nafion dispersion, the desired conducting powder, RuO_2, EmI-Tf, and isopropyl alcohol. This solution was sprayed directly onto each surface of the ionomer membrane in multiple layers. A very thin layer was applied to either side in succession, while the sample was continually rotated. The solvents were removed by heating the membrane under a heat lamp during the spraying process leaving a layer of conducting powder immersed in the now solidified Nafion, then annealed. After the application of the dispersion fluid, the sample was sandwiched between two 100 nm thin conductive gold foils and the three layers of the composite were fused together by a hot press at 160^{o} C at 550 psi for 15 seconds. For the proceeding experiments there were five different permutations used to determine how the electrode architecture and microstructure affect sensing, and these are summarized in Table 2.1. The generalization of thick and thin will be used since variability in the fabrication is inevitable. The thick samples were fabricated to be 20 μm and the thin 5 μm. The thickness was later quantified using a scanning electron microscope to determine each sample's respective geometries.

Table 2.1. Samples used in electrode study

	Ionomer thickness and loading			
Electrode	Thick 42% RuO_2 by volume	Thin 42% RuO_2 by volume	Thick 30% RuO_2 by volume	Thick 60% RuO_2 by volume
Thick	4	4	4	4
Thin	4	0	0	0

Multiple signal conditioners were tested to measure the current in the transducer. A two stage current amplifier, consisting of a transimpedance inverting input amplifier and a non-inverting voltage amplifier, was chosen for all tests as shown in Figure 2.1. The feedback loop in the first stage consisted of a metal film high precession resistor and was used to set the gain on the first stage. The resistor on the non-inverting input acted to decrease any bias current from the floating ground. By utilizing a two stage system, a reduced gain was set on each stage. With a lower gain on each stage, the bandwidth for the operational amplifier would be increased.

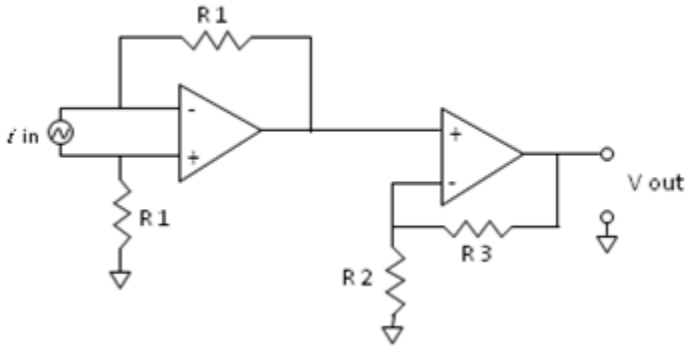

Figure 2.1 Schematic of the signal conditioner

Multiple operational amplifiers were tested to see which coupled the best with a high capacitance sensor. The IPMC sensor was placed in a clamped pinned configuration with a linear actuator driving the tip. The tip was perturbed with a sinusoidal input at 10 Hz. The corresponding voltage from the signal conditioner was measured using a National Instruments 6229 USB data acquisition system. The signal to noise ratio was taken at 10 Hz and was calculated using:

$$SNR = 10log_{10}\left(\frac{{V_{rms\ signal}}^2}{{V_{rms\ noise}}^2}\right)$$

where $V_{rms\ signal}$ is the root mean squared of a reconstructed signal at 10 Hz using the amplitude obtained by a normalized DFT at 10 Hz from the sensor, and $V_{rms\ noise}$ is the amplitude obtained by the normalized DFT at 10 Hz from the noise of the sensor. Since the traditional method to calculate the signal to noise ratio is based on bandwidth, the sampling rate would affect the apparent SNR. This was eliminated by restricting the bandwidth to the width of the bin of the DFT encompassing the driving frequency. The results can be seen in Figure 2.2 with Table 2.2 showing a comparison of some the properties of the various operational amplifiers.

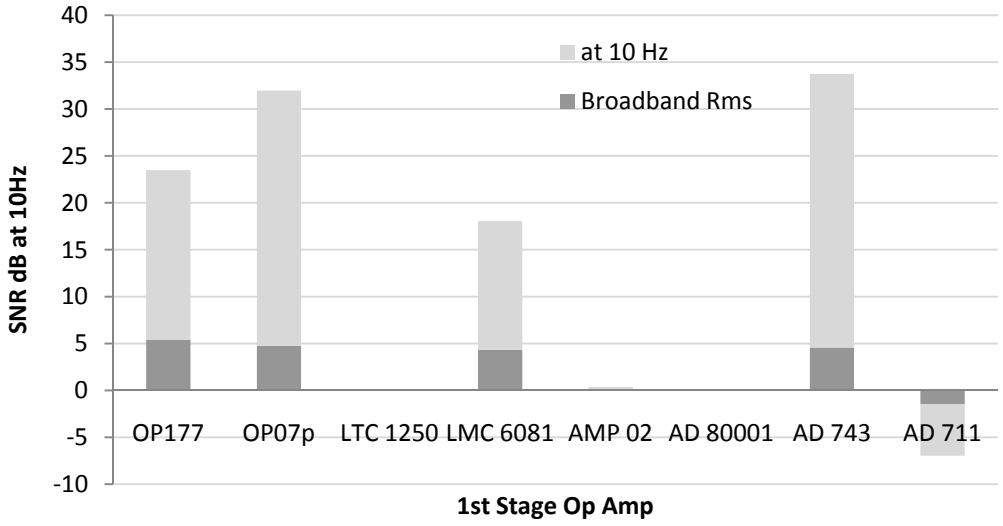

Figure 2.2 Signal to noise ratio at 10 Hz and broadband rms

Table 2.2. Specifications of the various test op amps

	Input Impedance	Slew Rate V/us	Vos uV	Input Noise a/rtHz	CMRR dB
OP 177	200 GΩ	0.3	10	11 nA	130
OP 07p	200 GΩ	0.08	30	6.6 pA	110
LTC 1250	NA	10	5	4 fA	130
LMC 6081	10 TΩ	1.5	150	22 nA	85
AMP 02	10 GΩ	6	200	9 nA	110
AD 80001	10 MΩ	1000	2000	2 pA	54
AD 743	3 TΩ	2.8	250	6.9 fA	95
AD 711	30 TΩ	20	200	.01 pA	88

From the above graph the ad743 exhibited the highest sensitivity with the OP07p and the OP177 in close proximity. Interestingly the AD743 did not have the highest input impedance, highest common mode rejection ratio, lowest slew rate, or voltage output offset. It did however have one of the lowest input noise values, but there were no clear trends among the properties to find an ideal operational amplifier for use with an IPMC with the above parameters. It is also interesting to note that the OP177 had the highest SNR when a bandwidth from 0 to 500 Hz was considered. This showed that despite its slightly lower gain, at 10 Hz the overall rms of the noise was lower than the OP07p. For broadband tests and transfer function calculations the OP177 was chosen for its lower broadband noise and high gain. The gain from the first stage multiplied by the gain from the second stage, yields the overall gain of the signal conditioner and is given by:

$$\frac{V_{out}}{i_{in}} = R_1\left(\frac{R_3 + R_2}{R_2}\right)$$

2.1.1 IMPEDANCE SPECTROSCOPY

Impedance spectroscopy is a method to interrogate object's electrical properties with the objective to understand its physical or chemical makeup. An impedance measurement is performed by applying a sinusoidal potential to an object and measuring the current response. The measurement takes the form:

$$Z(j\omega) = \frac{V(j\omega)}{I(j\omega)} = Z'(j\omega) + Z''(j\omega)$$

This can be performed at various excitation voltages, but typically it is kept low in order to ensure the input-output relationship is pseudo-linear. The impedance data for the fabricated samples was taken in a Faraday cage using an AutoLab PGSTAT100 potentiostat/galvanostat device seen in Figure 2.3.

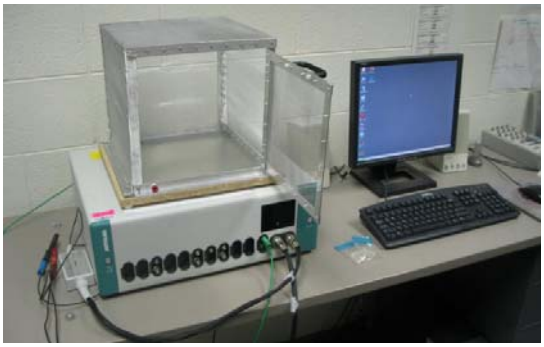

Figure 2.3 Autolab potentiostat/galvanostat. Photograph by Stephen Sarles 1/2/2008

A logarithmic sweep was used sampling 50 times from 1 MHz to 10 mHz using an excitation potential of 100 mV rms. The data was collected and examples are shown in Figure 2.4-2.8. Each figure shows a Bode plot of the acquired impedance data for samples 1-20. The impedance data became skewed at higher frequencies, therefore only the results up to 100 kHz were examined.

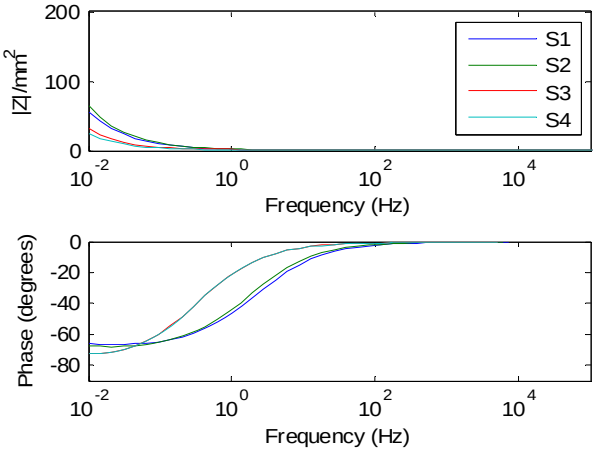

Figure 2.4 Bode plot of impedance data for group 1

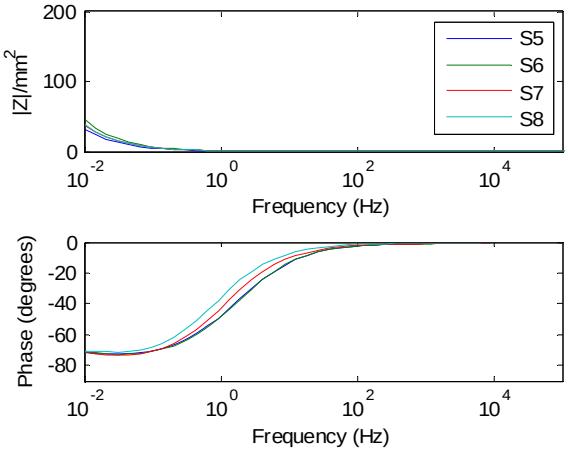

Figure 2.5 Bode plot of impedance data for group 2

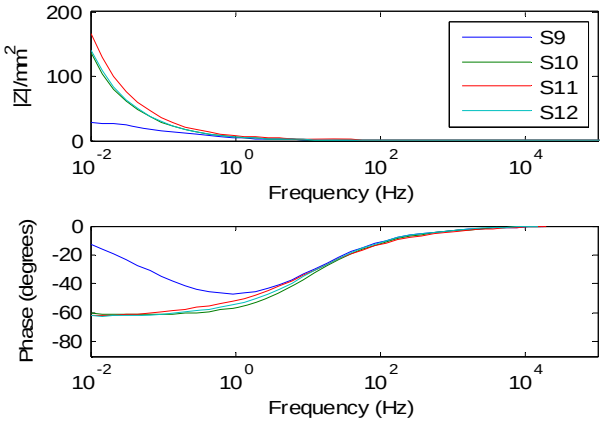

Figure 2.6 Bode plot of impedance data for group 3

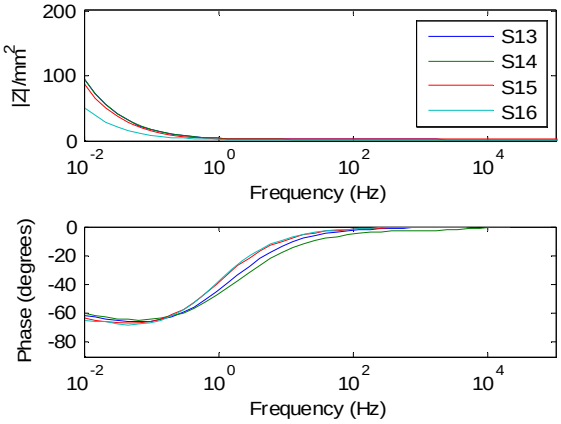

Figure 2.7 Bode plot of impedance data for group 4

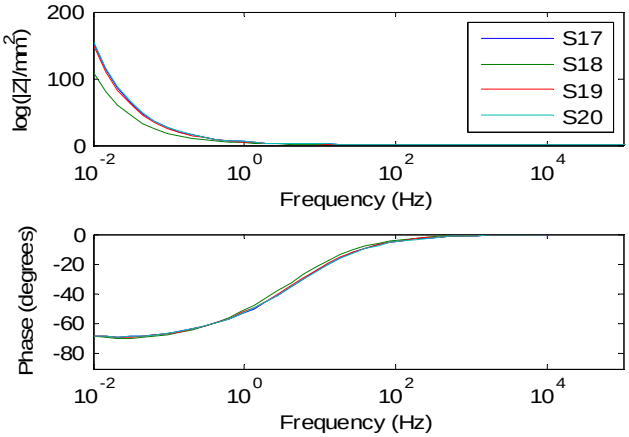

Figure 2.8 Bode plot of impedance data for group 5

Another way the impedance data was examined was to observe the Nyquist plot. Here the real and imaginary parts of the impedance were plotted on the x and y axis. The frequency was found by observing the angle from the origin to a given point on the Nyquist plot. The Nyquist plot was used in combination with the Bode plot to determine an equivalent circuit that fit the data. The Nyquist plots for the samples can be seen in Figure 2.9-2.13.

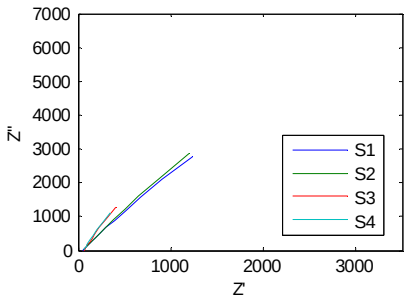

Figure 2.9 Nyquist for group 1

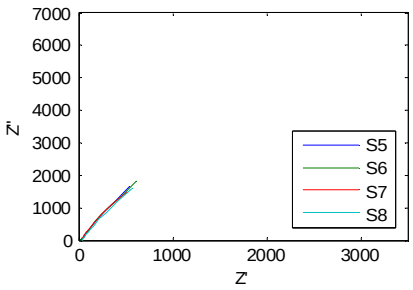

Figure 2.10 Nyquist for group 2

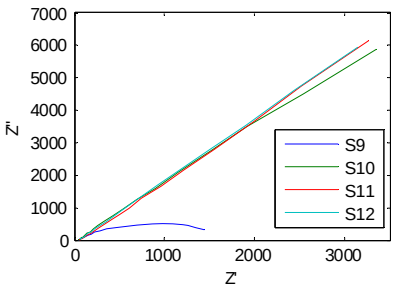

Figure 2.11 Nyquist for group 3

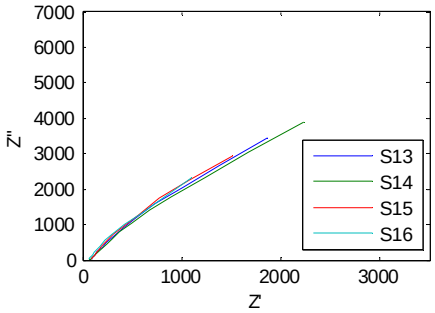

Figure 2.12 Nyquist for group 4

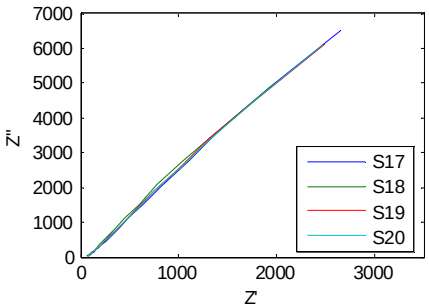

Figure 2.13 Nyquist for group 5

The capacitance has been calculated in multiple ways. Akle, in his study used the idea of the electrode acting as a capacitor, the ionomer as a resistor, and the adjacent electrode as a capacitor. This leads to a capacitance and resistance that are a function of frequency and take the form:

$$R(j\omega) = Z'(j\omega)$$

$$C(j\omega) = \frac{1}{j2\pi f Z''(j\omega)}$$

Solving for C and R and normalizing by the surface area of each transducer yields a frequency dependent capacitance and resistance seen in Figure 2.12-2.16. The capacitance and resistance values calculated came to an asymptote at approximately 1000 Hz.

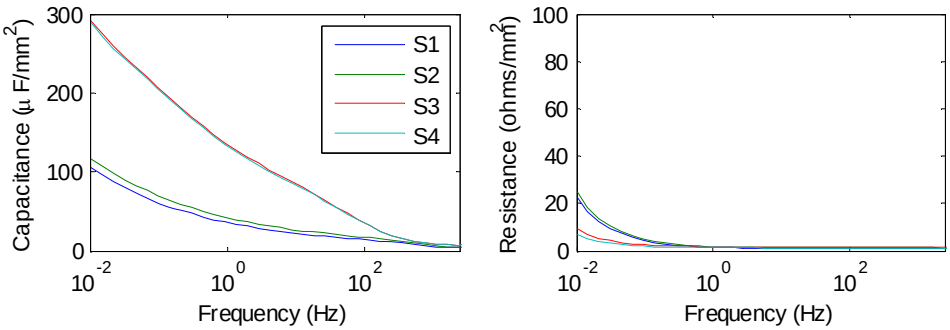

Figure 2.14 Capacitance and resistance for sensors in group 1

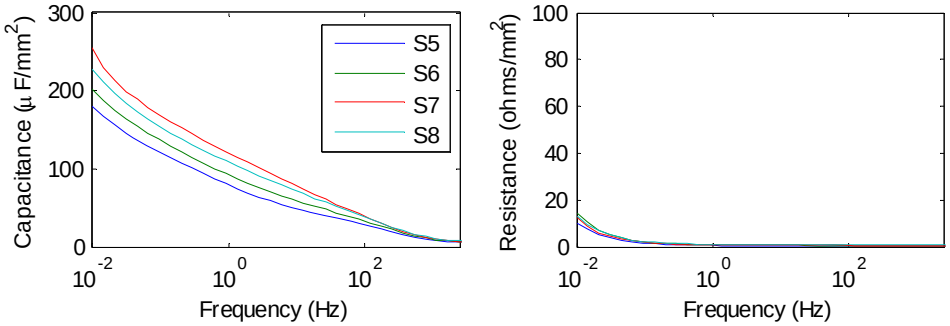

Figure 2.15 Capacitance and resistance for sensors in group 2

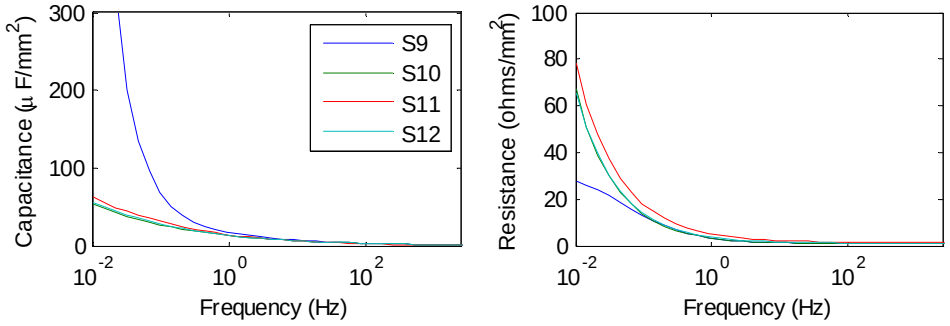

Figure 2.16 Capacitance and resistance for sensors in group 3

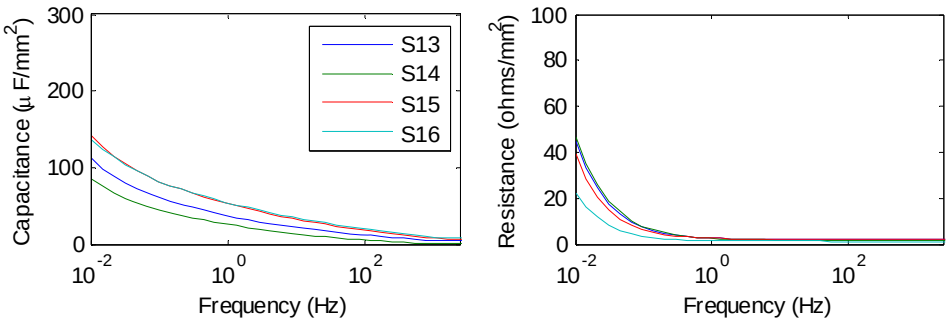

Figure 2.17 Capacitance and resistance for sensors in group 4

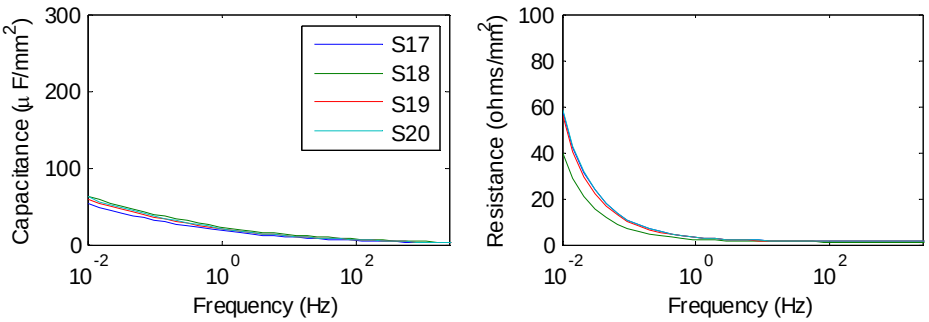

Figure 2.18 Capacitance and resistance for sensors in group 5

Observing the slope of the Nyquist plots, and the form of the Bode plots, the data lends itself to fit a Randle circuit. A Randle circuit is composed of three different electrical components, seen in Figure 2.19.

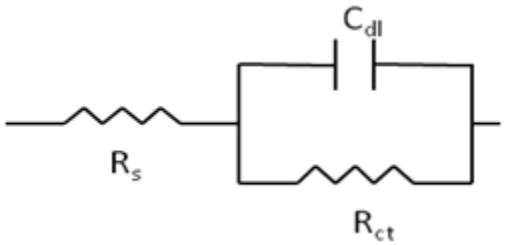

Figure 2.19 Ideal Randle circuit

The Randle circuit can be used to find the ionic conductivity resistance, R_s, the charge transport resistance, R_{ct}, and the charge carrying capability of an electric double layer, C_{dl}. This is an ideal

circuit to model the physical parameters within the electrode, and the ionomer independently. Previously Duncan introduced the charge transport resistance as the resistance associated with the interfacial boundary between the electrode and the ionomer [57]. Akle introduced the idea that the actuation was caused in part by the storage capacity of the electric double layer. Since an electric double layer will form around a conducting particle that is immersed in an ionic liquid, the Randle circuit is a reasonable circuit to use to model the transducer's impedance. The impedance data was fit in a similar way as Duncan [57]. The corresponding values for R_s, R_{ct}, and C_{dl} for all samples can be seen in Figure 2.20-2.22.

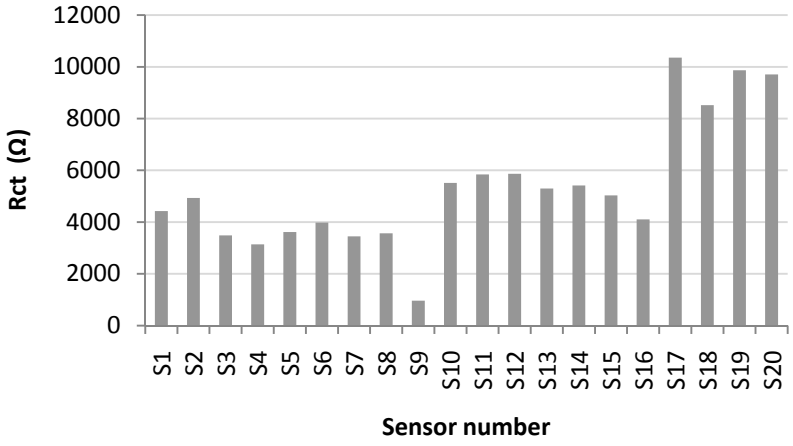

Figure 2.20 Calculated values on the charge transport resistance

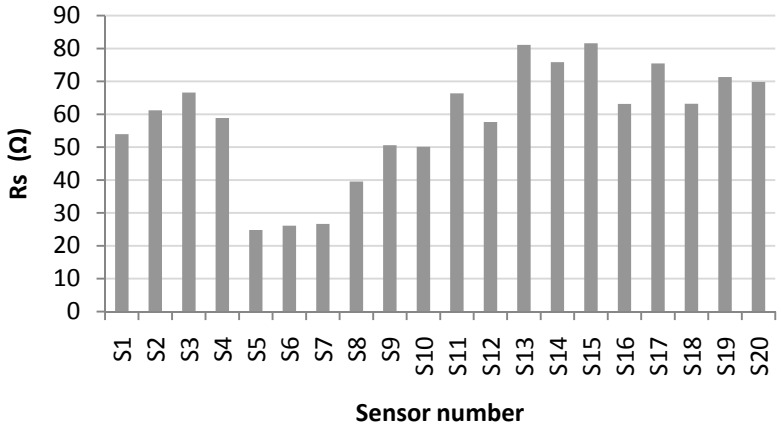

Figure 2.21 Calculated ionic conductivity values for all sensors

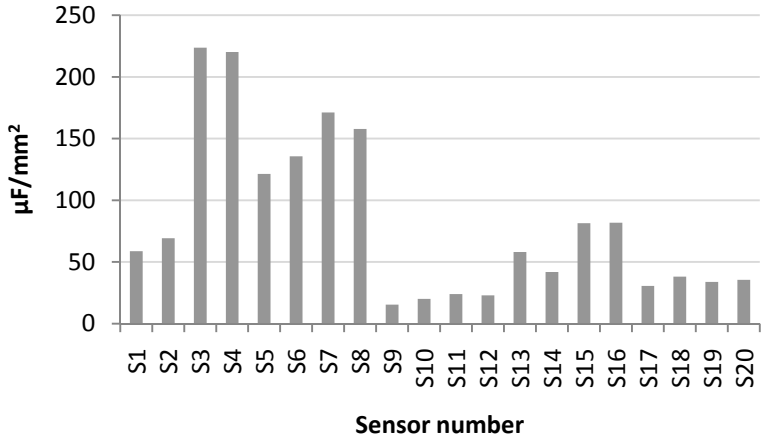

Figure 2.22 Calculated normalized capacitance values for all sensors

2.1.2 SCANNING ELECTRON MICROSCOPY

Another objective was to characterize the geometry of the transducer. Error from sample to sample was needed to estimate the error in manufacturing. The measurements were used to find the relation between the sensing mechanism and the physical geometry of the transducer. The physical geometry was also compared to the impedance data to find how to tailor the samples for sensing. The best way to determine the thickness and error was to take multiple

measurements through the thickness using a scanning electron microscope. For the following tests the FEI Quanta 600 FEG was used to image the cross section of all samples. Twenty samples were first frozen in liquid nitrogen and fractured to produce a clean edge to image. Using a sputter deposition, a 5 nm coating of gold was applied to all samples. The gold coating allows the ESEM to operate in a high vacuum mode, which yields higher signal to noise ratios for the images, resulting in sharp pictures, seen in Figure 2.23. Three regions, far left, middle, and far right of the sample were used to make measurements of the upper electrode thickness, the central ionomer thickness and the lower electrode thickness. Five measurements were taken for each of the three regions, for all three parts, for all twenty samples, equating to nine hundred measurements.

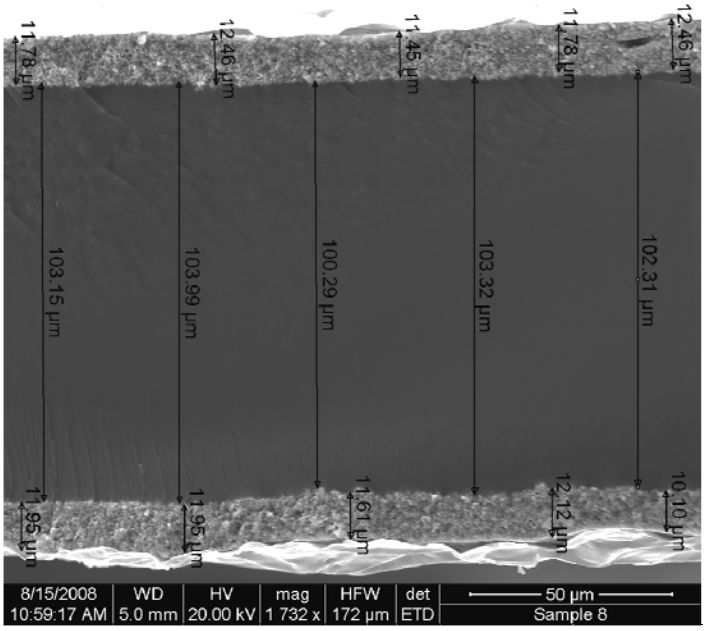

Figure 2.23 Typical image generated from the ESEM

The measurements for each of the electrodes and ionomers were tabulated. Figure 2.24 shows the mean value of the upper and lower electrode, with the error bars representing one

standard deviation of the measurements from the mean. The spraying process was done in such a way that the error can be assumed to have a normal distribution that is isotropic. Figure 2.25 shows the mean values for the ionomer and one standard deviation of the measurements from the mean. Figure 2.26 shows the deviation about the mean electrode thickness within a group. What can be concluded from the graph was the samples were all statistically similar within a group. In group one, two samples were similar, but drastically different from the other two in the same group, indicating an error within the sample set. The mean thicknesses of the electrodes for the thin samples were within 3 microns, and the mean of the electrodes were within the error of the adjacent side, again making them statistically similar and therefore assumed symmetric.

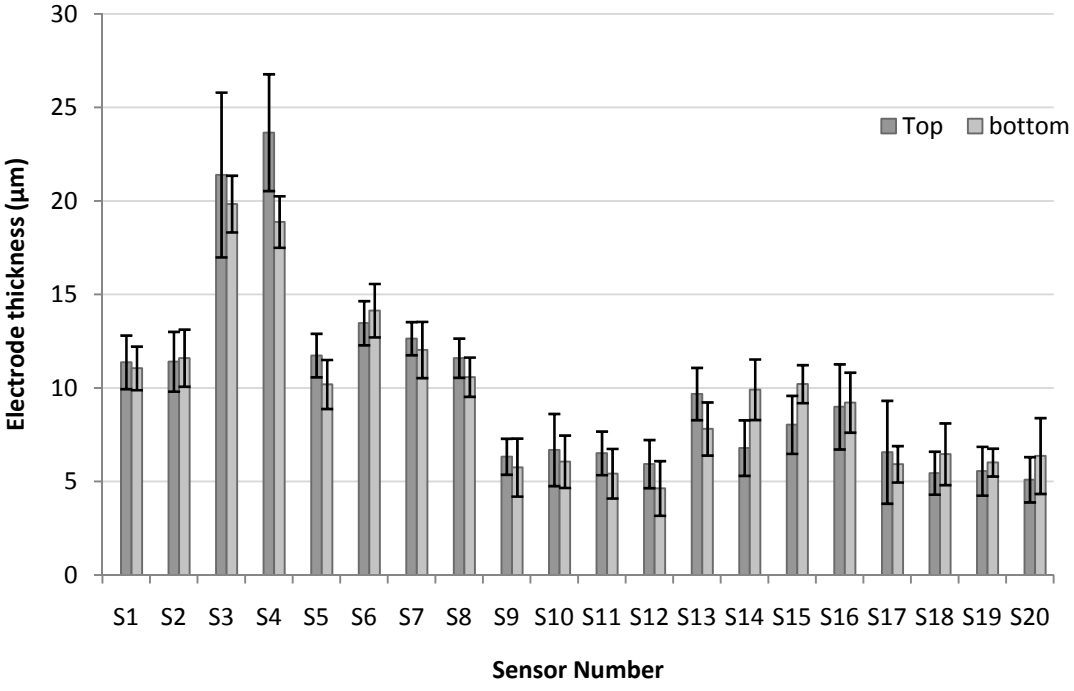

Figure 2.24 Comparison of the electrode architecture

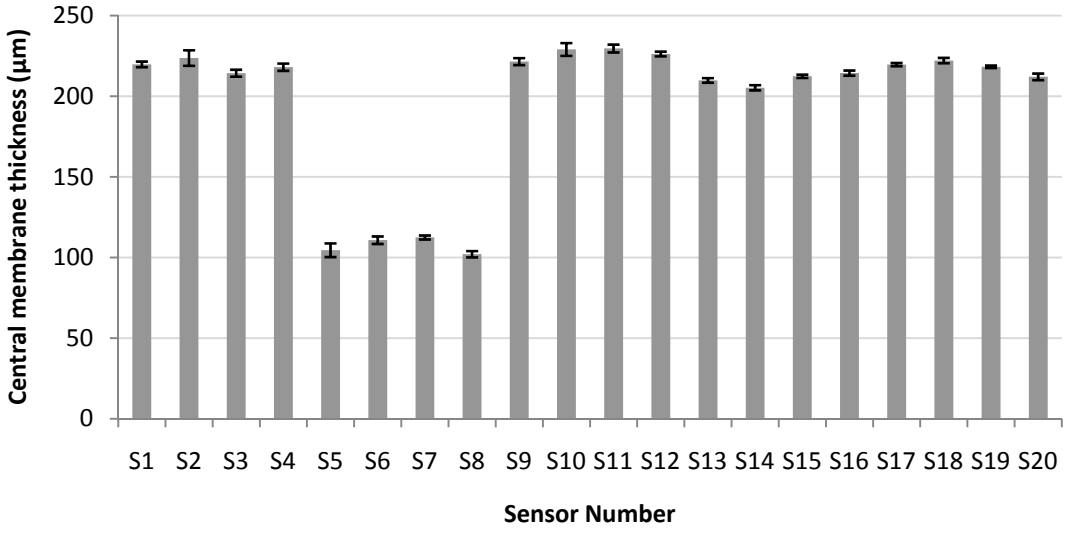

Figure 2.25 Comparison of the ionomer thickness

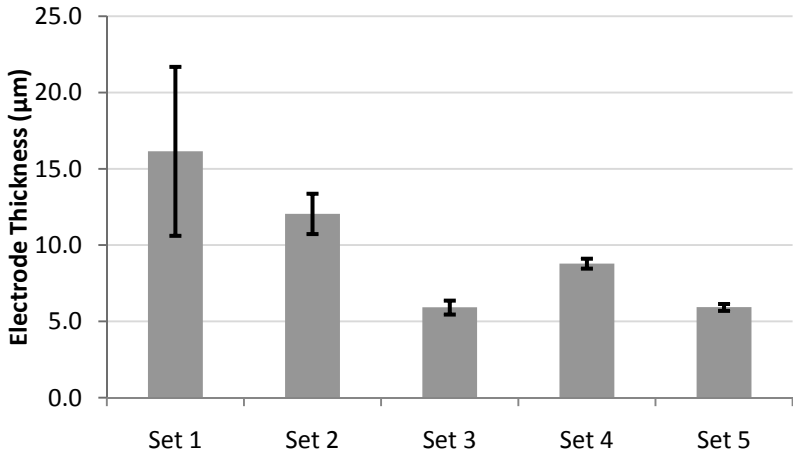

Figure 2.26 Deviation of the mean between the five sets

2.1.3 BENDING SENSITIVITY

The sensor needed to be isolated in a fixture that could accurately characterize the transducer's sensitivity to a displacement, when fixed in a cantilevered mode. A test fixture was developed to house an electromechanical shaker produced by Bruel and Kjaer Type 4810. The nylon tip of the shaker was adjusted to create a pre-stress in the transducer, which provided a restoring

force assuring the IPT stayed in contact with the shaker tip. Two separate tests were performed, one where the free length was 16 mm and one where the free length was 2 mm. With the free length set at 16 mm and a sample width of 1.6 mm, the electromechanical shaker was driven with a random signal ranging from .25 Hz to 100 Hz. The tip displacement was measured using a Polytec OFV-303 laser vibrometer with a sensitivity setting of 1280 µm/V with a noise floor at 20 mV. The current output from the transducer was measured using the aforementioned signal conditioner. A picture of the setup can be seen in Figure 2.27.

Figure 2.27 Bending test setup for a sensitivity comparison. Photograph by David Griffiths 2/22/2007

The next set of tests used a transducer with a fixed length of 2 mm to allow for actuation to higher frequencies, in order to determine the operational bandwidth of an IPT transducer. The sensitivity data was found by taking the quotient of the cross spectral density of the sensor's output and the laser vibrometer's output, and the power spectral density of the laser vibrometer's output. This gave a transfer function relating the voltage from the signal conditioner to the voltage of the laser vibrometer. This relation can be converted into a more usable form via:

$$\frac{V_{sensor}(\omega)}{\delta(\omega)} = \frac{V_{sensor}(\omega)}{V_{laser}(\omega)} \frac{1\ V}{G\ \mu m}$$

where G is the gain setting on the laser vibrometer. Another useful form was to calculate the strain energy in the electrode, assuming this was the active layer, and normalizing the sensitivity by this quantity. First, to calculate the strain energy a force balance was performed on a fixed cantilever beam to find the relation between force and displacement. This must be done since displacement was the measured variable. There was a resisting moment and a vertical force imposed at the tip from the shaker and can be modeled by:

$$EI \frac{d^2\delta}{dx^2} = F(L - x)$$

where E is the modulus of elasticity, I is the second area moment of inertia, F is the tip force, L is the length of the beam, δ is the transverse displacement, and x is a position along the beam. This can be solved by integrating twice and applying boundary conditions of dy/dx=0 at x=0, the fixed end, and y=0 at x=0. The displacement, δ, as a function of force takes the form:

$$\delta = \frac{FL^3}{3EI}$$

Next the strain energy was calculated. Strain energy is equal to the work [58] imposed therefore the strain energy, U can be defined as:

$$U = \int \frac{{\sigma_{11}}^2}{2E} dV$$

where σ_{11} is the stress in the 1-1 direction. σ_{11} for a cantilevered beam is defined as:

$$\sigma_{11} = \frac{My}{I} = \frac{FLy}{I}$$

where F is the force imposed on the tip, and y is the position in the beam from the neutral axis. Combining the previous equations the strain energy is defined as:

$$U = \int \frac{(FL)^2 y^2}{2EI^2} dV$$

Carrying out the integration and substituting displacement for force the strain energy can be defined as:

$$U = \frac{\delta^2 E T^3}{8L^2}$$

where T is the total thickness of the sample. This resulted in an expression for the total strain energy imposed to the sample given a measured displacement. However, since the electrode was assumed to be the active layer, the energy in the ionomer must be subtracted out. The strain energy in the electrode is:

$$U_{electrode} = \frac{\delta^2 E ({T_{total}}^3 - {T_{ionomer}}^3)}{8L^2}$$

The transfer function can be combined with this to find the sensitivity of the various transducers when normalized by the imparted strain energy.

$$\frac{V_{sensor}(\omega)}{U(\omega)} = \frac{V_{sensor}(\omega)}{\delta(\omega)^2} \frac{8L^2}{E({T_{total}}^3 - {T_{ionomer}}^3)}$$

All data sets were taken one step further to convert the voltage from the signal conditioner to a current by the previously derived relation to give the transfer function in units of Amps/Joule

and nA/µm. The transfer functions were compared at 30 Hz. The coherence between all sensitivity runs at 30 Hz was greater than 90%. There was also a discrepancy in the low frequency sensitivity between the like samples, but the deviation became less apparent past 10 Hz. The sensitivity was plotted for each sample in their respective groups for the twenty transducers, seen in Figure 2.28 and Figure 2.29.

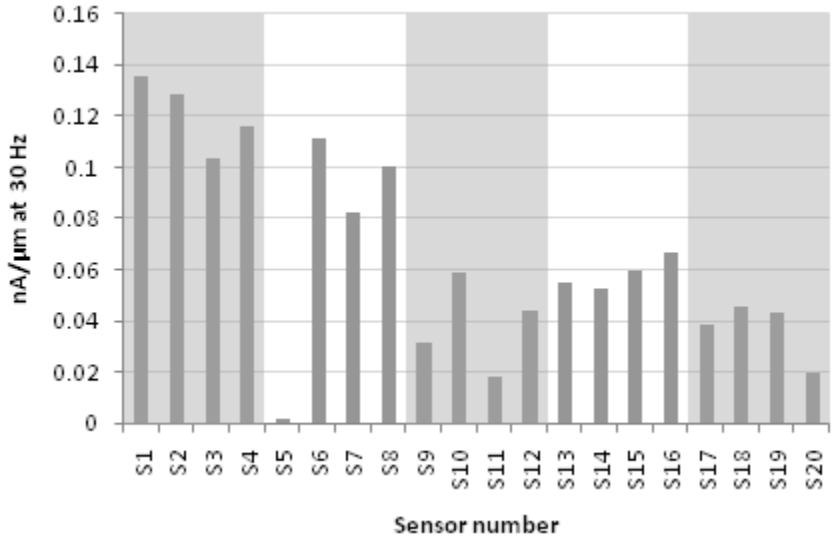

Figure 2.28 Sensitivity at 30 Hz with respect to tip displacement of the transducer

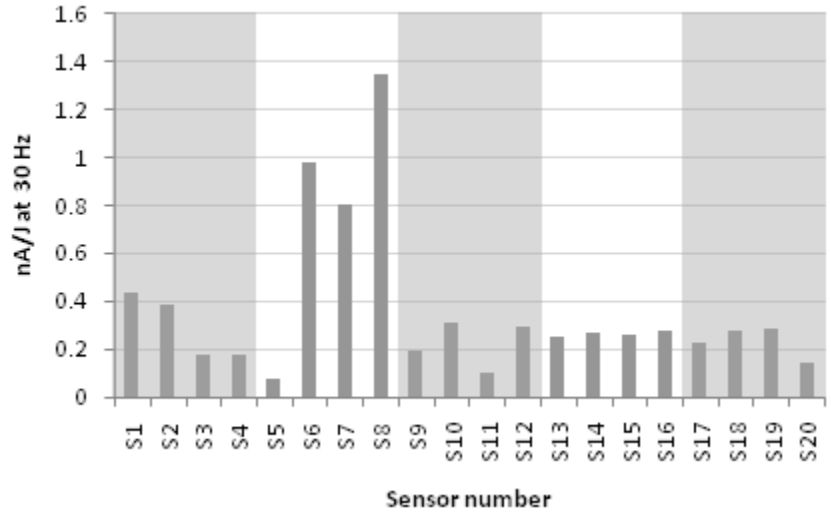

Figure 2.29 Sensitivity at 30 Hz with respect to strain energy

The second set of tests, with the decreased free length, was used to determine the bandwidth of the transducer. For this test the 2 mm free length sample was used again with the tip displacement measured using the laser vibrometer with varying gain which ranged from 1280 µm/V to 80 µm/V, which allowed for a resolvable displacement down to 1.6 µm. Because there is a decrease in amplitude of the shaker's output with an increase in frequency, the response of the transducer at high frequencies has not been previously measured. To date, the fastest response was reported by Buechler at 500 Hz. An initial test using the traditional method of applying a white noise over the .25 to 2 kHz bandwidth was performed and can be seen in Figure 2.30. In order to resolve the high frequency data, the gain on the laser vibrometer must be changed to a higher sensitivity, with an increase in frequency, and the driving input current must be increased to get a higher displacement. With an increase in current to the shaker, the electromagnetic field strength increases, this can manifest itself as noise in the sensor output and appear as a false positive result. This was tested by retracting the shaker tip until it no longer touched the transducer and was actuated. The spectral content from the output of the unactuated transducer was calculated and if there was any energy at the operational frequency of the shaker it was considered noise and a false positive result. The noise was found to begin manifesting itself at 4 kHz, therefore tests up to 2 kHz were reported. However, 2 kHz is still 4 times greater than previously recorded, and the tests show no sign of a roll off. Due to the need to change the gain of the laser vibrometer for the higher frequencies, the data must be acquired and processed differently. Multiple tests were performed by running the transducer at a discrete frequency for 30 seconds. For each test the frequency of the shaker was increased and the gain on the laser vibrometer increased. The transfer function

and coherence was calculated for each run and reassembled. The reassembled transfer function showed a smoothed version of the transducers frequency dependent sensitivity. One underlying assumption that must be verified to credit the validity of the discrete transfer function analysis is the linearity of the response with displacement. This was checked by driving the shaker at different amplitudes and calculating the transfer function. The system was found to be linear as all the calculated transfer functions converged despite the magnitude of the input, seen in Figure 2.30.

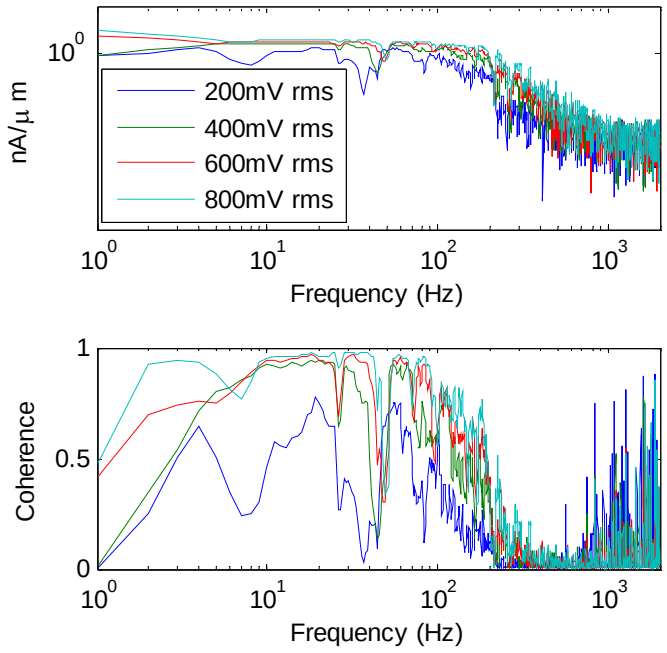

Figure 2.30 Calculated transfer function and coherence for a single sample with varying amplitudes

The discrete transfer function routine started at .1 Hz and extended through 2 kHz with one 30 second measurement, sampled at 6 kHz, for 10 points per decade. The output from the discrete transfer function can be seen in Figure 2.31, along with the coherence. The two methods were overlaid with the measurements in Figure 2.32 from the broadband input, to

show the similarity between the two and the effectiveness of the method to resolve high frequencies.

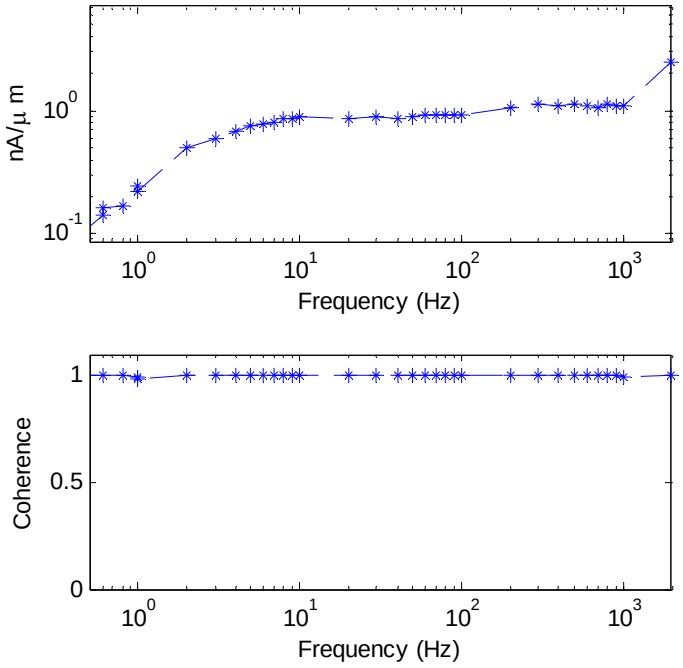

Figure 2.31 Transfer function and coherence of the discrete method

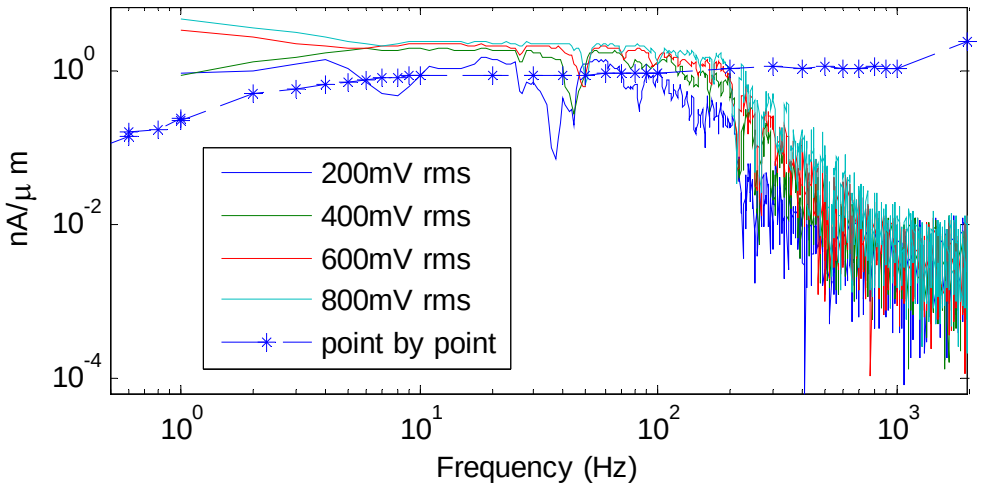

Figure 2.32 The discrete transfer function overlaid with white noise input method

2.2 RESULTS

The primary goals of performing the impedance tests were to find how the geometry affects the sensitivity, the electrical properties affect the sensitivity, and what properties of the IPMC can be altered to increase the transducers ability to sense an outside perturbation. From the raw impedance data, sensitivity data, and SEM's, six of the twenty samples were deemed damaged during the characterization process and omitted for the following analysis. First the electrical properties were examined and related to sensitivity, and then the electrical parameters were related to the physical parameters. All sensitivities were reported purely from an input to output perspective, where a mechanical displacement was the input and a current was the output. Figure 2.33 shows the relation between the electric double layer capacitance and the sensitivity of the transducer. Similar to what Akle has reported for actuation, there was a linear relationship between the sensing performance and the capacitance associated with the electric double layer. Figure 2.34 shows the relation between the ionic conductivity and the sensitivity. Interestingly there was a lack of a trend, signifying that ionic conductivity was not directly proportional to the sensitivity. In Figure 2.35 a comparison between the charge transfer resistance, or interfacial resistance, and the sensitivity shows there was approximately a power law governing the sensitivity.

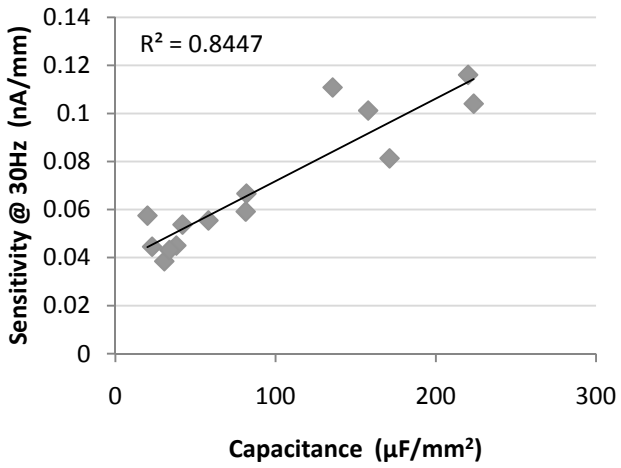

Figure 2.33 Relation between the electric double layer capacitance and sensitivity

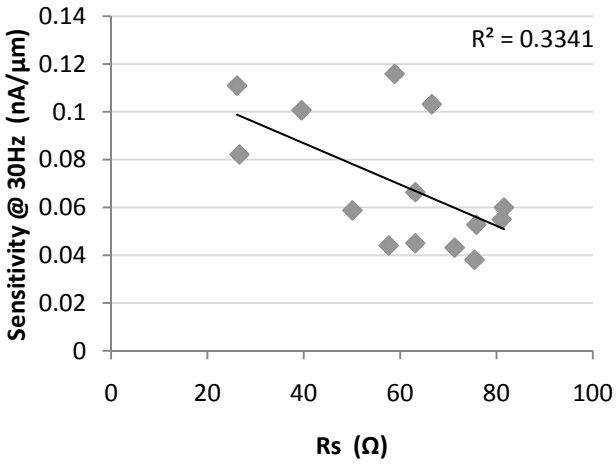

Figure 2.34 Relation between ionic conductivity resistance and sensitivity

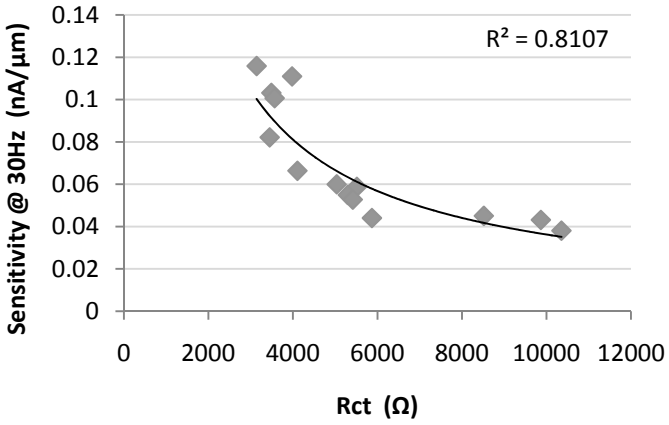

Figure 2.35 Relation between charge transport resistance and sensitivity

Next the relation between the physical architecture and the electrical parameters were compared. The relation between the electric double layer capacitance and the electrode geometry was linear, seen in Figure 2.36, yielding the conclusion that the capacitance was directly proportional to the volume of the electrode. If the capacitance was equivalent to a parallel plate capacitor the capacitance would only be a function of area. Figure 2.37 shows a relation between the absolute capacitance and the expected volume of conducting powder,

proving the measured capacitance must be caused by the formation of an electric double layer about the conducting particles.

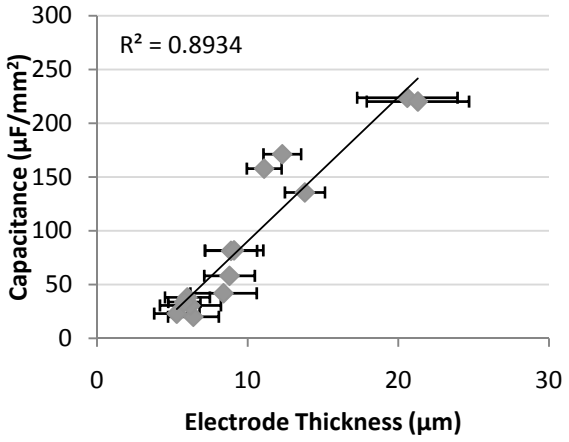

Figure 2.36 EDL capacitance and electrode thickness

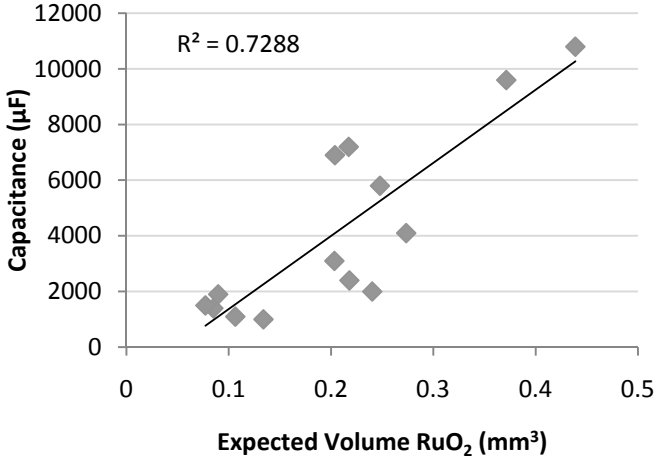

Figure 2.37 EDL capacitance and volume of conducting powder

Next the relation between the ionomer thickness and electrode thickness was related to the ionic conductivity resistance seen in Figure 2.38 and Figure 2.39. Here a wide range of ionic conductivity resistance values were measured for electrode thickness's indicating there was not a substantial relation between the two. When the ionic conductivity resistance was plotted against the ionomer thickness a sharp drop in the conductivity was observed. The ionic conductivity resistance was therefore a measure of the resistivity of the path a charged particle must travel, which agreed with Farinholt's previous findings.

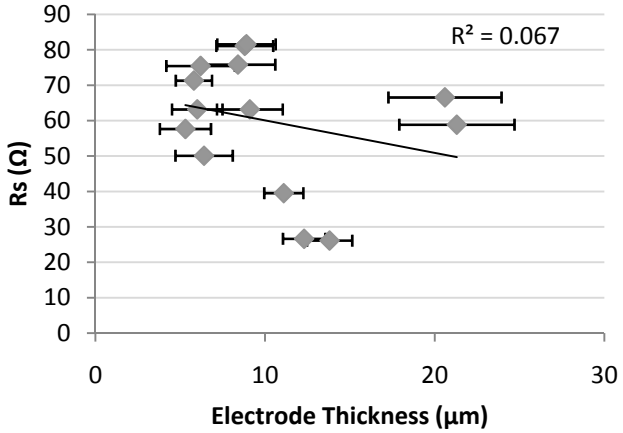

Figure 2.38 Ionic conductivity and electrode thickness

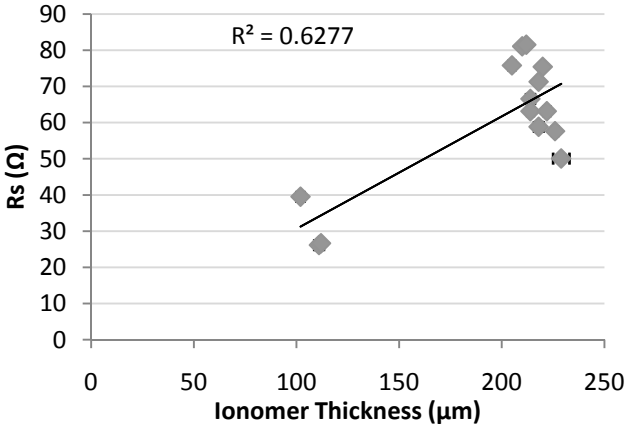

Figure 2.39 Ionic conductivity and ionomer thickness

Finally the relation between the charge transfer, or interfacial resistance, was examined with regard to the physical geometry. Figure 2.40 and Figure 2.41 show their relation to the electrode architecture and the ionomer architecture. Here an emergence of a power relation was observed indicating the charge transfer resistance, or interfacial resistance was a property associated with the electrode and its formation. When the sensitivity was normalized by the work into the electrode an increase in sensitivity was observed with a decrease in the ionic conductivity resistance and decrease in ionomer thickness, seen in Figure 2.42 and Figure 2.43.

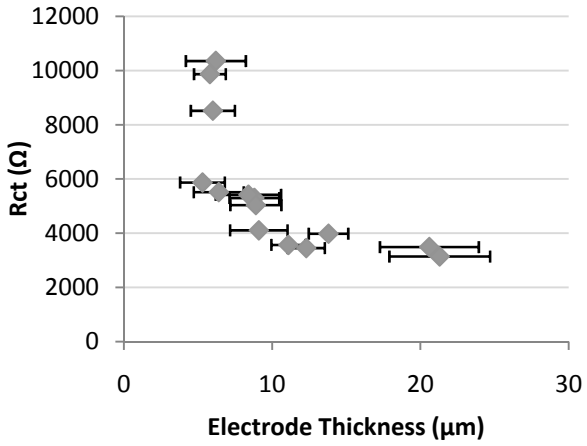

Figure 2.40 Charge transport resistance to electrode thickness

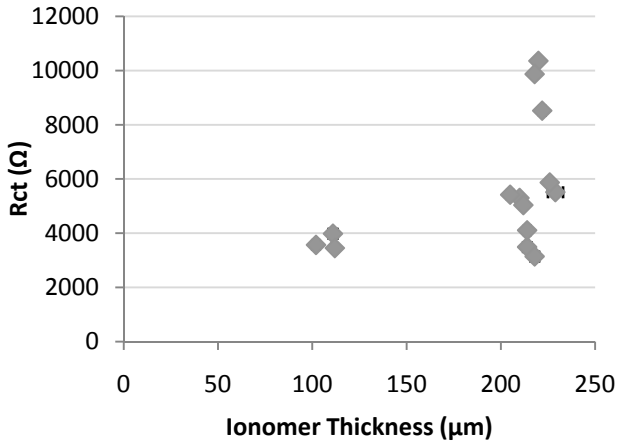

Figure 2.41 Charge transport resistance to ionomer thickness

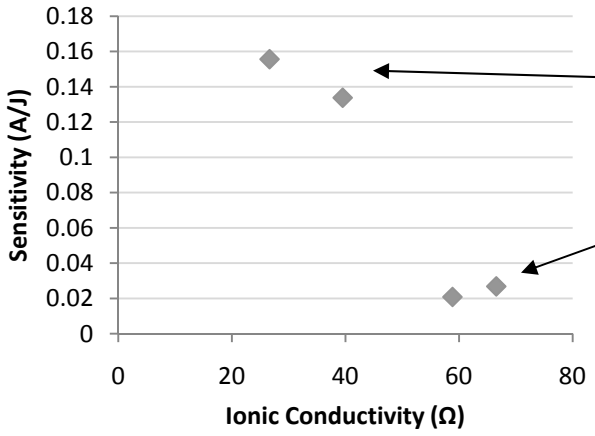

Figure 2.42 Sensitivity per unit work compared to ionic conductivity

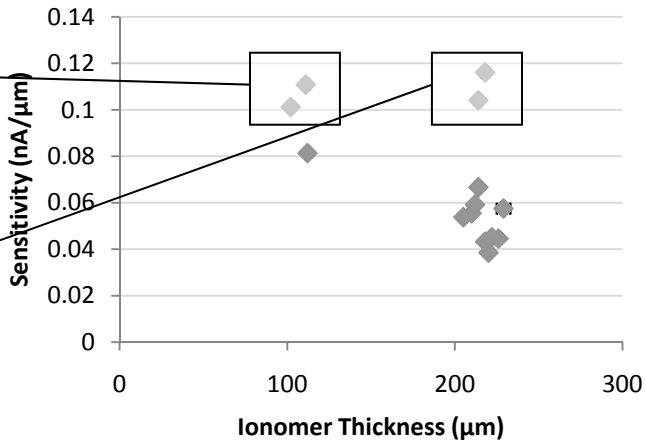

Figure 2.43 Sensitivity per unit work compared to ionomer thickness

2.3 CONCLUSION

In this section twenty transducers were fully characterized by their electrical properties, physical properties, and electrical response. By looking purely at an input output relation the electric double layer capacitance was linearly proportional to the sensitivity of the transducer. The capacitance was also found to be proportional to the volume of the conducting particles. This indicated the measured capacitance must be caused from an electric double layer formation about the conducting particles and was one process involved in the transduction mechanism. It was also found that a reduction in the interfacial resistance increased the sensitivity. It was possible to reduce the ionic conductivity resistance by reducing the thickness of the central ionomer. Reducing the ionic conductivity resistance tended to enhance the current output for a given unit of work into the electrode. This indicated the central layer of the composite dictated the energy conversion efficiency, whereas manipulation of the electrode altered sensitivity. An analogy can be drawn between an IPT and an electric double layer super capacitor (EDLC). An EDLC is built with a central membrane designed to inhibit the

flow of charge. The IPT transducer has a similar inhibiting device as the central ionomer that resisted charge migration under steady state conditions, which allowed for a storage potential within the electrodes. When an outside source of energy was imparted to the transducer it forced a discharge from the capacitive layers, similar to what Newbury modeled.

CHAPTER 3 DEVELOPMENT OF A BIO-ACOUSTIC SENSOR

INTRODUCTION

Auscultation has been an integral part of medical diagnostics for many years, and hit its peak with the invention of the stethoscope in 1816 by French physician Rene Theophile Hyacinthe Laennec. The first stethoscope was made from three pieces of wood, two hollow cylinders and a cone attachment [59]. It was modified into a trumpet shape in 1828 by Pierre Piorry, and was called the monaural stethoscope. In 1855, Dr. George Cammann introduced the binaural stethoscope, giving it multiple earpieces. The most commonly used stethoscope today is the binaural stethoscope with a bell and diaphragm chest piece. This design originated in 1926 by Howard Sparque and its design has remained almost unchanged. The latest advance in this technology came in the form of an electronic stethoscope, created by Amplivox in 1961. Since this time many variants of both the traditional binaural stethoscope and electronic stethoscope have been developed. Despite its invention over 45 years ago, the electronic stethoscope primarily remains an academic tool. The electronic stethoscope, unlike the traditional stethoscope, allows the physician to acquire acoustic pressure waves for quantitative analysis and nearly real-time unbiased diagnostics of cardiovascular conditions. Despite the lengthy service of the traditional stethoscope, its effectiveness has recently come under scrutiny [60]. The ability to accurately resolve and identify all of the cardiac and respiratory sounds through auscultation is prone to error [61]. A new emphasis has emerged for the advancement of the electronic stethoscope and predictive algorithms to remove the guesswork associated with traditional auscultation.

There are two primary methods to sense pressure wave propagation in the body, either through an air coupled system or a direct contact system. The air coupled systems were the first systems to be developed, but are prone to outside noise contamination of the desired signal. An air coupled system is an electronic microphone that has been embedded in the transmission line that would traditionally go to the physicians ears. Another factor hindering air coupled systems is the acoustical impedance mismatch between air and skin, which allows less than 1% of the total energy to propagate outside of the skin [62]. Multiple configurations of contact type electronic stethoscopes have been developed to avoid the impedance mismatch, many using either a fixed reference [63, 64], or an inertial reference [65] to get a transducer to produce a voltage or current that is proportional to the incident pressure wave. Many of these devices have shown success in detection of the S1 and S2 cardiac sounds as well as other cardiac sounds [63, 64]. A major disadvantage of the current systems is their inability to resolve low frequencies. Many of the cardiac sounds have been classified as having spectral content from 20 to 250 Hz [66], but few of the electronic stethoscopes can actually resolve frequencies below 20 Hz. This area is particularly important because it is below the audible threshold. Here a new variant of the electronic stethoscope is introduced that can resolve frequencies below 1 Hz and over 500 Hz by capitalizing on the flexibility and high sensitivity of an ionic polymer metallic composite.

3.1 DESIGN OF A BIO-ACOUSTIC SENSOR

There are multiple configurations that can be utilized to detect pressure waves in the body. The configuration chosen has the IPT oriented as a cantilever beam in a fixed pinned configuration, shown in Figure 3.1. The diaphragm has been selected for an acoustic impedance match and low surface density to ensure transmission of the acoustic energy from the body to the sensing element. The same two stage current to voltage and voltage to voltage amplifier was used.

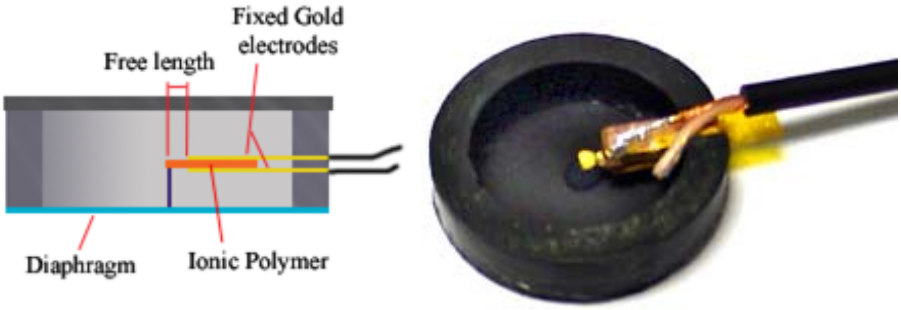

Figure 3.1 Cross section of the cantilevered configuration, and actual picture with the wiring exposed

The dynamics of the system were based on the deformation of the diaphragm under an applied acoustic pressure field that was coupled to a sensing element. The resultant force due to the deformation of the IPT was considered negligible since it was on the order of micro Newtons. The diaphragm was modeled as a plate because the restoring force was assumed to only be a function of the tension in the diaphragm and not the stiffness of the material. This allowed the diaphragm to be modeled as a circular plate fixed at the rim. The displacement, $\Psi(r)$, at any point on the plate was solved using the radial 2-d wave equation:

$$\Psi(r) = \frac{P}{T}\left[\frac{J_0(kr) - J_0(kR)}{k^2 J_0(kR)}\right]$$

where P is the incident pressure, T is the initial tension in the membrane, k is the angular wave number, r is the radial position of interrogation, and R is the radius of the diaphragm. Damping can be accounted for by the introduction of a complex wave number. The IPT was characterized in a cantilevered configuration to find the transfer function empirically for the voltage output from the signal conditioner per radian of rotation, seen in Figure 3.2.

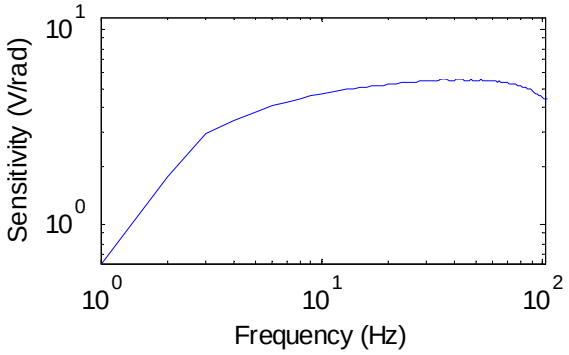

Figure 3.2 Sensitivity per unit radian

Combining these equations with the empirical transfer function yielded a predicated voltage output for a given design at any given frequency. The geometric parameters, and conditions were optimized using a genetic algorithm to determine what features should be maximized or minimized for the greatest response to cardiac sounds. The optimization showed the diameter of the diaphragm should be maximized, the surface density minimized, the free length minimized and the pretension minimized, but high enough to keep the resonance out of the bandwidth of interrogation. The final design used in this experiment had a diaphragm diameter of 27 mm, a free length of 2 mm, a pretension of approximately 1 mN/m, and a surface density

of 1.9 kg/m^2. The predicted sensitivity for the bio-acoustic sensor was calculated using the relation for center displacement and the measured transfer function, seen in Figure 3.3.

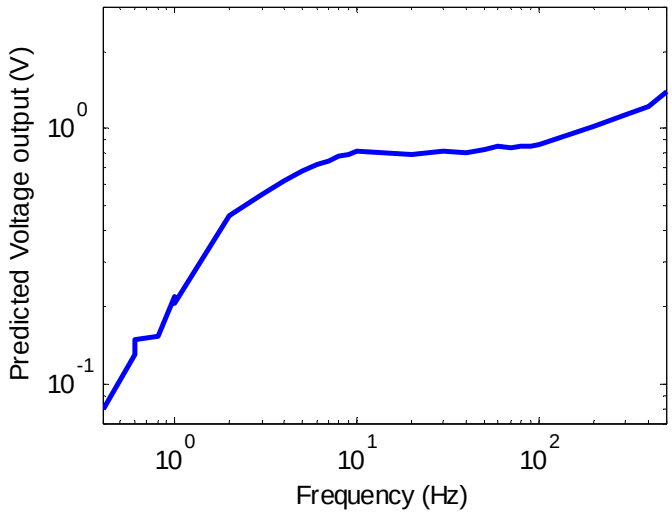

Figure 3.3 Predicted center displacement for a reference pressure of 1 Pa

3.2 TESTING AND VALIDATION OF THE BIO-ACOUSTIC SENSOR

A bio-acoustic transducer was fabricated based upon the previous analysis. It was tensioned by axially stretching the membrane over a large tube and fixing it at the corners. The bio-acoustic sensor was fixed to the stretched membrane then cut from the tube. It was used to acquire both the arterial pressure wave and the acoustic emissions from the thorax. The following will show the results from the bio-acoustic sensor and compare them to a commercially available 3M Littman 3000 electronic stethoscope.

ACQUISITION OF CAROTID PRESSURE WAVE

The ability to accurately resolve the pressure wave amplitude and pressure wave speed of the carotid pressure is widely thought to be a good predictor of the vessel compliance and health

[67]. The first test performed was on the carotid artery, since stiffening of the carotid artery can be a warning sign for a stroke. The IPT based electronic stethoscope was placed on the subject's right carotid artery and lightly held in place. The pressure waveform was recorded for ten seconds and sampled at 1 kHz using a 12 bit USB DAQ from National Instruments. The total time series can be seen in Figure 3.4, showing the repeatability of the measurement. Figure 3.5 shows three such cycles where both the systolic and diastolic pressures are seen. The systolic is highlighted in light gray and the diastolic in dark gray. The classic arterial pressure waveform has a pulse duration of 0.8 seconds, with the systolic cycle accounting for about 35% of the duty cycle and the remaining 65% corresponding to the diastolic cycle. The output showed approximately 30% duty cycle on the systolic cycle and 70% corresponding to the diastolic cycle. Considering this is a comparison of an idealized case to empirical data, the two waveforms are very similar. The dichrotic notch was also observed, which signified an increase in pressure in the aorta and showed the closing of the aortic valve. Such a device can also be easily used to measure heart rate and rhythm using a proper algorithm to process the data.

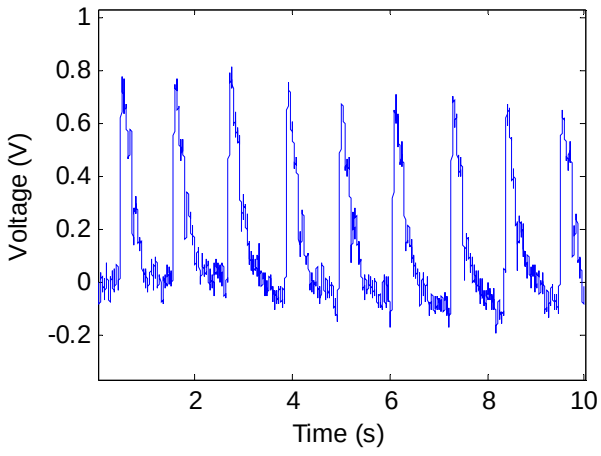

Figure 3.4 Unfiltered time series of the pressure waveform

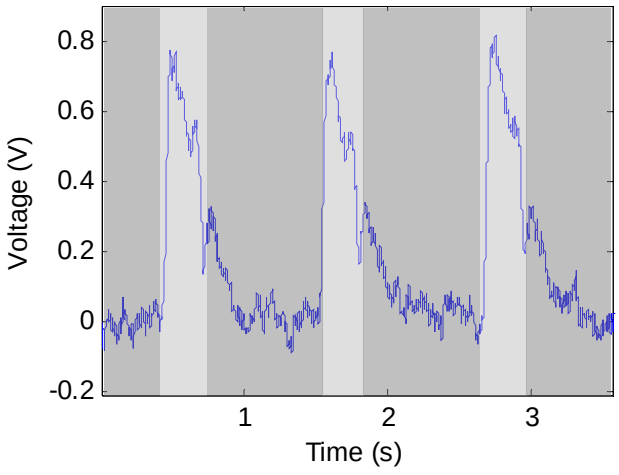

Figure 3.5 Three cycles distinguishing the systolic and diastolic phase

The cardiac pressure wave was initially measured using the same IPT based stethoscope for 4 seconds using a 12 bit USB DAQ from National Instruments at 1024 Hz. Later a similar waveform was acquired using a 3M Littman 3000 electronic stethoscope. The acquired waveforms were read in through a computer's sound card, sampling at 8000 Hz with 16 bit resolution and was down sampled to 1024 Hz. The power spectral density of both signals were calculated in order to see periodicities, utilizing 4096 points in the Fourier transform yielding a frequency resolution of .25 Hz via the Welch method seen in Figure 3.7 and Figure 3.7.

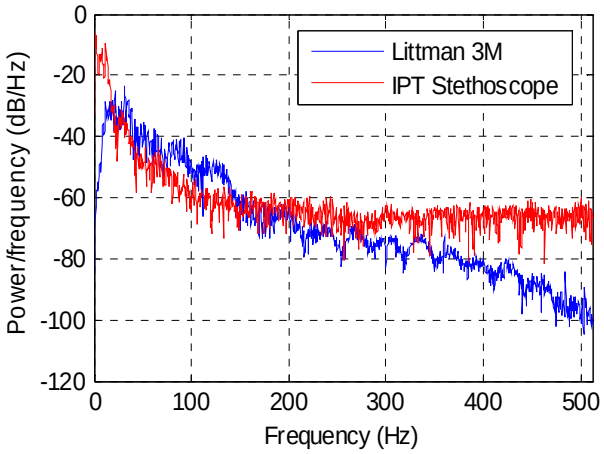

Figure 3.6 Comparison of the power spectral density's over the entire bandwidth

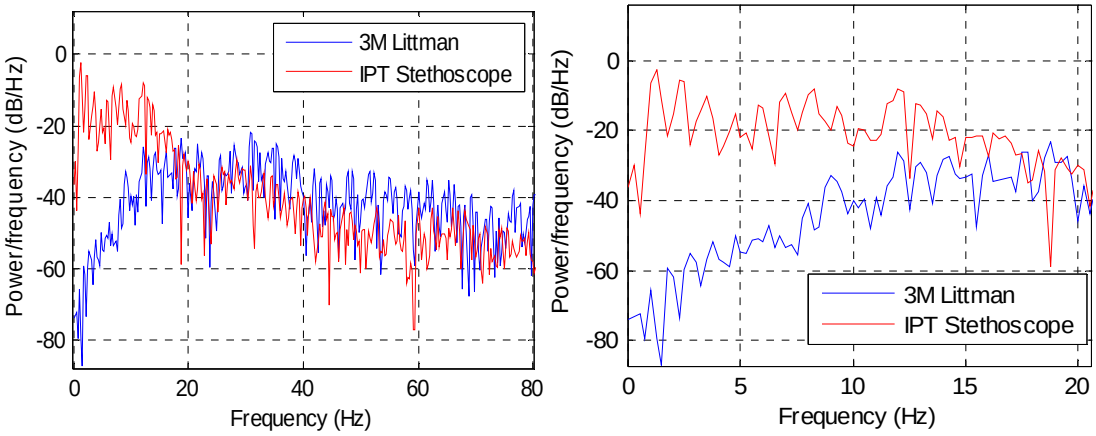

Figure 3.7 Comparison of signal power in the in the low to infrasonic bands

A Fourier transform was used to get a comparison between the magnitudes of the raw voltage signals. This was used as a basis to see what frequency domain the IPT can be improved, and where the IPT excels when compared to a commercial option, seen in Figure 3.8.

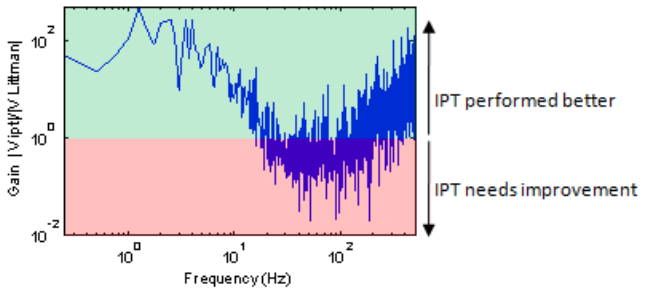

Figure 3.8 Difference in gain in the magnitude of the voltage within their frequency band

A spectrogram was used to illustrate the sounds and their similarities, seen in Figure 3.9 and Figure 3.10. The spectrogram used a short time Fourier transform with a window length of .125 seconds and a frequency resolution of .5 Hz using 90% overlap. A majority of the power in the acquired waveform from the IPT based stethoscope for the S1 and S2 sounds was observed below 110 Hz, with lower power extending up to 500 Hz which was consistent with previous work [68] and the Littman. However, the 3M Littman exhibited a greater response in the band of 100 to 300 Hz when compared to the IPT based stethoscope. The dominant frequencies in the PSD of the IPT based stethoscope were found to be 1 Hz and 2 Hz, which corresponds to the occurrence of the S1 and S2 phenomena. High energy content was also observed in the spectral realm of 5 to 15 Hz, which is not audible to the human ear, and is believed to correspond to arterial or venous pulses [68]. Interestingly similar energy content was observed

by the 3M, but nearly 100 times lower in amplitude. As per the manufacturers specifications the high pass roll off of the 3M is at 20 Hz.

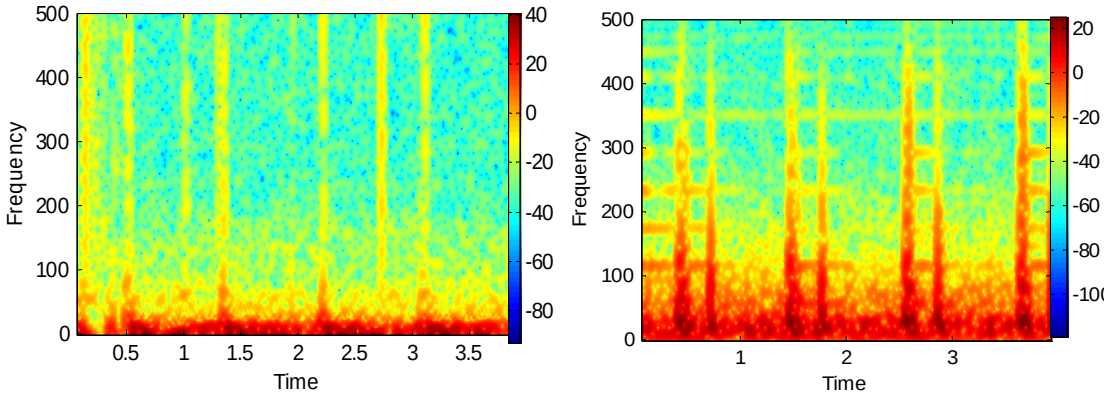

Figure 3.9 Left. Spectrogram from the IPT based stethoscope over the compete bandwidth. Right. Spectrogram from the 3M. Both showing 4 cycles

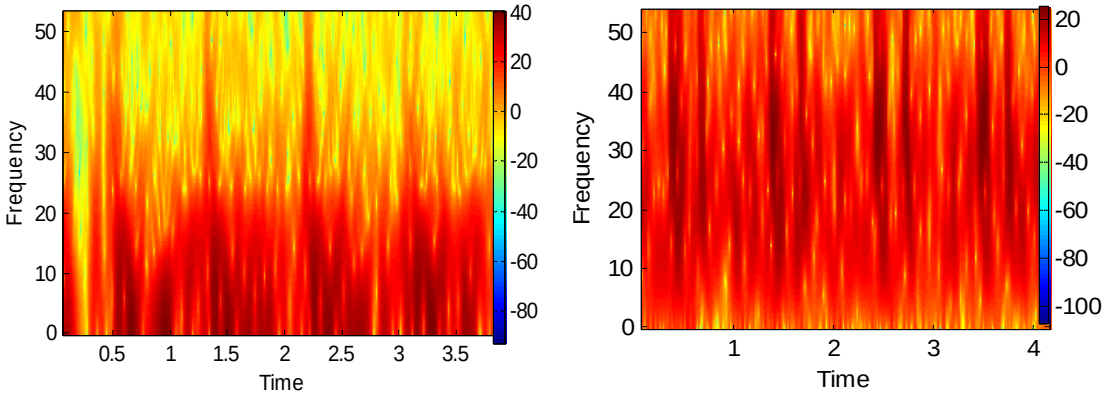

Figure 3.10 Left. Spectrogram from the IPT based stethoscope for infrasonic. Right. Infrasonic and low frequency shown from the 3M

3.3 CONCLUSION

Presented in this chapter was the foundation for the development of an electronic stethoscope utilizing an ionic polymer metallic composite configured in a cantilever configuration. This was the first sensor of its kind that has been demonstrated to work in situ. Both the arterial

pressure wave and the cardiac bio-acoustics were successfully captured. Both the systolic and diastolic cycles were observed in the arterial waveform. The dichrotic notch was clearly observable, signifying the closing of the aortic valves. It was found that the IPT based sensor has a much higher sensitivity to the infrasonic than a standard commerical electronic stethoscope. It was also observed that the commercial stethoscope performed slightly better in the low frequency realm of 20 to 200 Hz. From the data obtained from the IPT based electronic stethoscope it is clear that modern auscultation methods are inadequte when it comes to the infrasonic, and different methods must be developed. The greatest power within the aquired waveform was in the infrasonic realm, demonstrating its need to be studied.

CHAPTER 4 CONCLUDING REMARKS AND FUTURE RECOMMENDATIONS

In this document the history and current development of ionic polymer metallic composites has been presented. The review indicated an emphasis on modeling the transducer, with negligence on a full characterization and implementation of an IPT as a sensor. This document covered a complete study of the electrodes and the ionomer, their architecture, electrical properties and the effect they have on sensing. In a previous study Akle introduced the idea of an electric double layer formation about the conducting particles creating a means for charge storage, and showed a correlation between capacitance and the actuation performance of an IPT. This study was built on the ideas brought forth by Akle to explore the metrics that dictate the sensitivity of an IPT when used in a sensing mode. A series of impedance tests were performed to prove the sensitivity of the transducer was proportional to the measured electric double layer capacitance, seen in Figure Figure **4.1**. A linear relation was observed between the expected volume of the conducting powder and the capacitance, indicating the volume of the conducting powder will alter the charge storage ability, seen in Figure Figure 4.2.

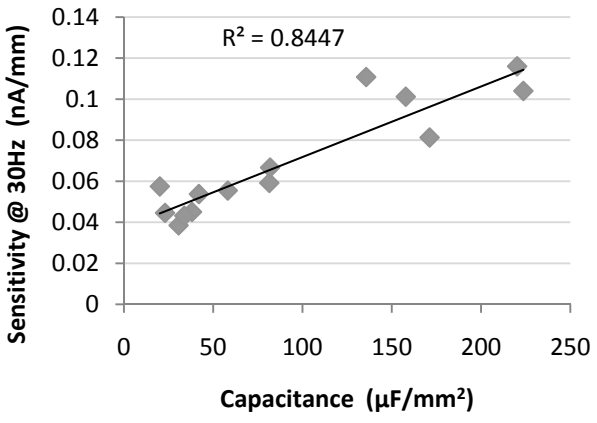

Figure 4.1 Sensitivity compared to the measured electric double layer capacitance

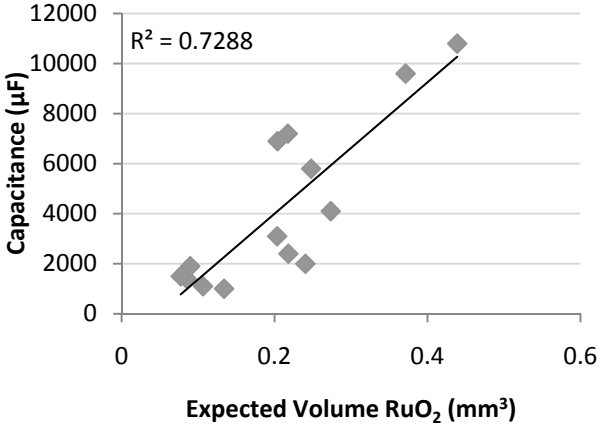

Figure 4.2 Electric double layer capacitance compared to expected RuO_2 volume

The ionic conductivity resistance was found to be independent of the sensitivity of the transducer. However, it was found to enhance the energy conversion from mechanical to electrical energy. Figure Figure **4.3** demonstrates this idea by showing a comparison between four transducers with similar sensitivities, despite the first two transducers having nearly 25% lower charge storage capabilities. The ionic conductivity resistance was shown to be geometrically dependent on the thickness of the central membrane. This result indicated the ionic conductivity resistance was analogous to the path the charge must travel, and as the length of that path increased, the electrical, and mechanical resistance to the flow of charge increased, seen in Figure Figure **4.4**.

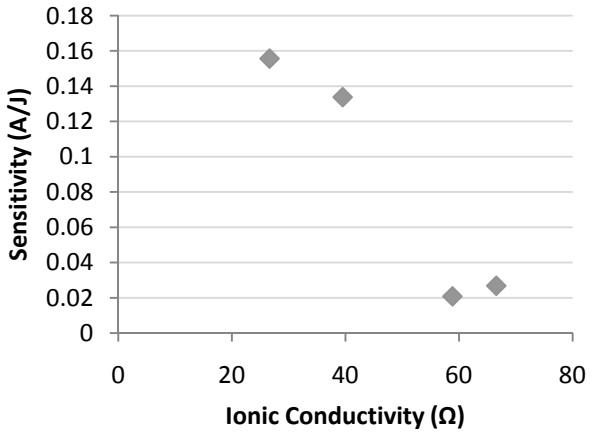

Figure 4.3 Comparison of mechanical work to electrical current for transducers of similar sensitivity and varying charge storage capacity

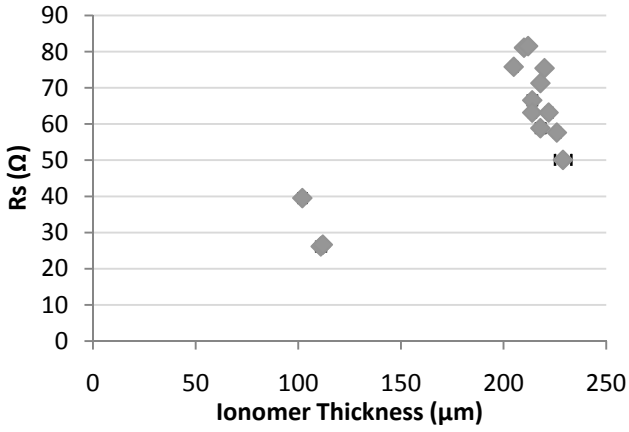

Figure 4.4 Ionic conductivity compared to ionomer thickness

The sensitivity was also linked to the interfacial resistance of the applied electrode layer and the central ionomer. The interfacial resistance should be reduced as much as possible in order to increase the transducers sensitivity. A few causes for an increase in the interfacial resistance were found from delamination of the various layers or a poor merger of the two layers. The

interfacial resistance can be compared to a thermal contact resistance, where a poor or incomplete union between the central membrane and the electrode would add an electrical resistance. From the measured samples the interfacial resistance appeared to reach a minimum value of 3.4 kΩ, seen in Figure Figure 4.5. This result indicated the interfacial resistance should be reduced as much as possible, however will hit a limit which was dictated by the fabrication of the transducer. Therefore this measurement may be used to investigate the quality of the fabricated transducer. An ionic polymer metallic composite was also characterized for the first time up to 2 kHz, seen in Figure Figure 4.6. The results indicated an increase in sensitivity with frequency, with no signs of a maximum limit.

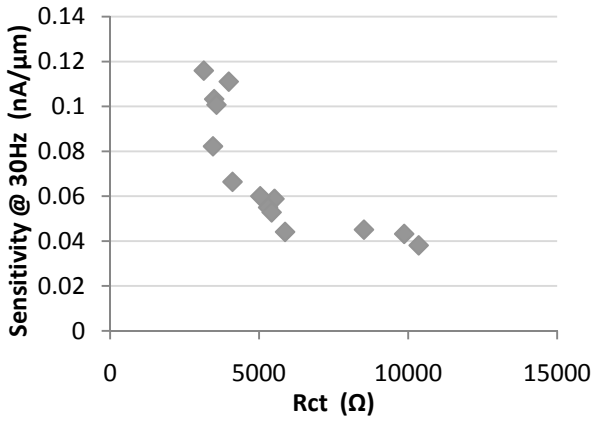

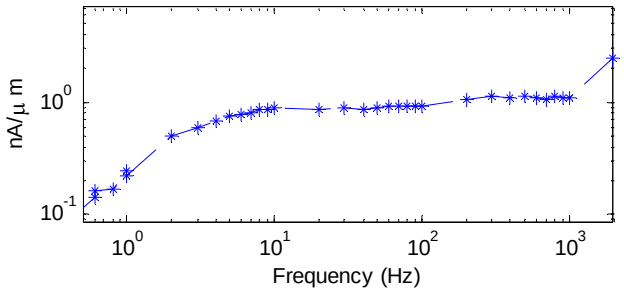

Figure 4.5 Sensitivity compared to interfacial resistance **Figure 4.6** Bending sensitivity of a 2 mm cantilevered IPT

To prove the viability of an IPT as a sensor that can compete with a commercial technology, a bio-acoustic sensor was developed. This was one of the first IPMC based transducers that showed a clear advantage over a currently commercialized sensor. The bio-acoustic sensor was designed to operate in the 0,0 mode below 500 Hz. The IPT was fixed to the center of an impedance matched membrane to transmit the acoustic energy to the IPT. An IPT was fabricated based on the previous analysis to have a high electric double layer capacitance, low

interfacial resistance and low ionic conductivity resistance. The bio-acoustic sensor was shown to be able to resolve both the arterial wave form, and cardiac sounds emanating from the body, seen in Figures Figure 4.7 and Figure 4.8.

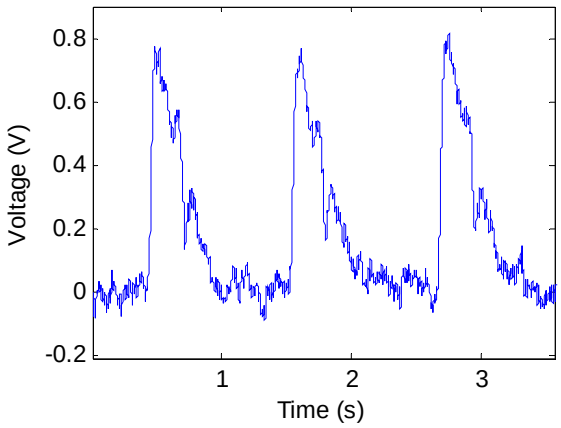

Figure 4.7 Acquired arterial pressure waveform

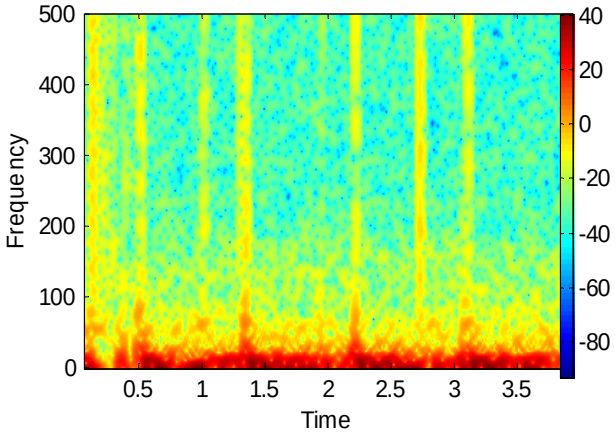

Figure 4.8 Acquired cardiac sounds

When the bio-acoustic sensor was compared to the output from a 3M Littman electronic stethoscope, an increase in energy within the infrasonic bandwidth was observed. This was accomplished by utilizing the quasi-static sensitivity of an IPT and applying it to a fixture that was designed for the absorption of acoustic energy.

Based upon the results concluded from this work, IPT's are a new and promising technology that can be utilized effectively as sensors. However, before significant progress can be made, further investigation of the transduction mechanism is required on multiple length scales. With a better understanding of the fundamental physics and driving mechanism, further improvements can be made to the fabrication process and selection of materials. The effects of the central ionomer are not yet fully understood. A study on the central ionomer with varying cluster morphology should be investigated to observe the effects on the sensitivity and efficiency of the transducers.

ACKNOWLEDGMENTS

Throughout my graduate experience at Virginia Tech I feel very fortunate to have been given the privilege to work among some very talented and selfless individuals. I would like to begin by thanking Dr. Pavlos Vlachos for the opportunities that he provided for me throughout my graduate experience. I would also like to thank Dr. Barbar Akle of the Lebanese American University for the personal time he took to provide technical insight and support. I'd also like to acknowledge my colleague Andy Duncan for his patience and the hours he spent explaining polymer science to a mechanical engineer. I would like to thank the corner crew, Dave Hubble, Chris Weiland, and Andy Gifford for their advice and assistance, as well as Dan Cooper for his assistance with the acoustics and the rest of my colleagues in the AEThER lab. Lastly I would like to thank my Mom, Patricia Griffiths, Dad, John Griffiths, and Sister, Laura Griffiths, for their never ending support.

BIBLIOGRAPHY

1. Kuhn, W., et al., *Reversible Dilation and Contraction by Changing the State of Ionization of High-Polymer Acid Networks.* Nature, 1950. **165**(4196): p. 514-516.

2. Katchalsky, A., *Rapid swelling and deswelling of reversible gels of polymeric acids by ionization.* Cellular and Molecular Life Science, 1948. **5**(8): p. 319-320.

3. Hamlen, R.P., C.E. Kent, and S.N. Shafer, *Electrolytically Activated Contractile Polymer.* Nature, 1965. **206**(4989): p. 1149-1150.

4. Osada, Y. and M. Hasebe, *Electrically activated mechanochemical devices using polyelectrolyte gels.* Chemistry Leters, 1985. **14**(9): p. 1285-1288.

5. Grodzinsky, A.J. and J.R. Melcher, *Electromechanical Transduction with Charged Polyelectrolyte Membranes.* IEEE Transactions on Biomedical Engineering, 1976. **BME-23**(6): p. 421-433.

6. Yannas, I. and A. Grodzinsky, *Journal of mechanochemistry and cell mortility*. 1973.

7. Oguro, K., Y. Kawami, and H. Takenaka, *Bending of an ion-conducting polymer filmelectrode composite by an electric stimulus at low voltage.* Journal of the Micromachine Society, 1992. **5**: p. 27-30.

8. Shahinpoor, M., *Conceptual design, kinematics and dynamics of swimming robotic structures using ionic polymeric gel muscles.* Smart Materials and Structures, 1992. **1**(1): p. 91-94.

9. Sadeghipour, K., R. Salomon, and S. Neogi, *Development of a novel electrochemically active membrane and 'smart' material based vibration sensor/damper.* Smart Materials and Structures, 1992. **1**(2): p. 172.

10. Duncan, A.J., D. Leo, and T. Long, *Beyond Nafion: Charged Macromolecules Tailored for Performance as Ionic Polymer Transducers.* Macromolecules, 2008. **accepted/in press**.

11. Wallmersperger, T., D.J. Leo, and C.S. Kothera, *Transport modeling in ionomeric polymer transducers and its relationship to electromechanical coupling.* Journal of Applied Physics, 2007. **101**(2): p. 024912/1-024912/9.

12. Newbury, K.M. and D.J. Leo, *Linear constitutive model of ionic polymer bender transducers*, in *Proceedings of SPIE-The International Society for Optical Engineering*. 2003. p. 88-99.

13. Farinholt, K.M. and D.J. Leo, *Electromechanical modeling of charge sensing in ionic polymers*, in *Proceedings of SPIE-The International Society for Optical Engineering*. 2003. p. 13-24.

14. Newbury, K.M. and D.J. Leo, *Electromechanical Modeling and Characterization of Ionic Polymer Benders.* Journal of Intelligent Material Systems and Structures, 2002. **13**(1): p. 51-60.

15. Chen, Z., et al., *A dynamic model for ionic polymer-metal composite sensors.* Smart Materials and Structures, 2007. **16**(4): p. 1477-1488.

16. Takenaka, H., et al., *Solid polymer electrolyte water electrolysis.* International Journal of of Hydrogen Energy, 1982. **7**: p. 397-403.

17. Millet, P., M. Pineri, and R. Durand, *New solid polymer electrolyte composites for water electrolysis.* Journal of Applied Electrochemistry, 1989. **19**: p. 162-166.

18. Akle, B.J., et al., *Effects of electrode morphology on the performance of BPSH and PATS ionic polymer transducers*, in *Proceedings of SPIE-The International Society for Optical Engineering*. 2004. p. 413-424.

19. Akle, B.J., et al., *Correlation of capacitance and actuation in ionomeric polymer transducers.* Journal of Materials Science, 2005. **40**(14): p. 3715-3724.

20. Kim, K.J. and M. Shahinpoor, *Effect of the surface-electrode resistance on the actuation of ionic polymer-metal composite (IPMC) artificial muscles*, in *Proceedings of SPIE-The International Society for Optical Engineering*. 1999. p. 308-319.

21. Shahinpoor, M. and K.J. Kim, *The effect of surface-electrode resistance on the performance of ionic polymer-metal composite (IPMC) artificial muscles.* Smart Materials and Structures, 2000. **9**(4): p. 543-551.

22. Bennett, M. and D. Leo, *Morphological and electromechanical characterization of ionic liquid/Nafion polymer composites*, in *Proceedings of SPIE-The International Society for Optical Engineering*. 2005. p. 506-517.

23. Griffiths, D., et al., *Development of ionic polymer transducers as flow shear stress sensors: Effects of electrode architecture*, in *Proceedings of SPIE-The International Society for Optical Engineering*. 2007. p. 65290L/1-65290L/9.

24. Chung, C.K., et al., *A novel fabrication of ionic polymer-metal composites (IPMC) actuator with silver nano-powders.* Sensors and Actuators, B: Chemical, 2006. **B117**(2): p. 367-375.

25. Kim, K.J. and M. Shahinpoor, *A novel method of manufacturing three-dimensional ionic polymer-metal composites (IPMCs) biomimetic sensors, actuators and artificial muscles.* Polymer, 2001. **43**(3): p. 797-802.

26. Kim, K.J. and M. Shahinpoor, *Development of three-dimensional polymeric artificial muscles*, in *Proceedings of SPIE-The International Society for Optical Engineering*. 2001. p. 223-232.

27. Akle, B., et al., *Direct assembly process for fabrication of ionomeric polymer devices*. 2006, (USA). Application: US. p. 30pp.

28. Griffiths, D., et al. *Micro deposition method: a novel fabrication method for ionic polymer metallic composites*. 2008: SPIE.

29. Nemat-Nasser, S. and J.Y. Li, *Electromechanical response of ionic polymer metal composites*, in *Proceedings of SPIE-The International Society for Optical Engineering*. 2000. p. 82-91.

30. Nemat-Nasser, S. and J.Y. Li, *Electromechanical response of ionic polymer-metal composites.* Journal of Applied Physics, 2000. **87**(7): p. 3321-3331.

31. Newbury, K. and D.J. Leo, *Modeling of electromechanical transduction in ionic polymer materials*, in *AD (American Society of Mechanical Engineers)*. 2002. p. 47-57.

32. Newbury, K.M. and D.J. Leo, *Linear Electromechanical Model of Ionic Polymer Transducers -Part I: Model Development.* Journal of Intelligent Material Systems and Structures, 2003. **14**(6): p. 333-342.

33. Farinholt, K. and D.J. Leo, *Modeling of electromechanical charge sensing in ionic polymer transducers.* Mechanics of Materials, 2004. **36**(5-6): p. 421-433.

34. Buechler, M.A. and D.J. Leo, *A variational model of ionomeric polymer actuators and sensors*, in *Proceedings of SPIE-The International Society for Optical Engineering*. 2005. p. 118-129.

35. Buechler, M.A. and D.J. Leo, *Characterization and Variational Modeling of Ionic Polymer Transducers.* Journal of Vibration and Acoustics, 2007. **129**(1): p. 113-120.

36. Konyo, M., et al., *Development of velocity sensor using ionic polymer-metal composites*, in *Proceedings of SPIE-The International Society for Optical Engineering*. 2004. p. 307-318.

37. Pudipeddi, A., D. Kim, and K.J. Kim, *Sensory behavior of ionic polymer metal composite*, in *Proceedings of SPIE-The International Society for Optical Engineering*. 2006. p. 61681Y/1-61681Y/10.

38. Bonomo, C., et al., *A model for ionic polymer metal composites as sensors.* Smart Materials and Structures, 2006(3): p. 749.

39. Shahinpoor, M., et al., *Sensing capabilities of ionic polymer-metal composites*, in *Proceedings of SPIE-The International Society for Optical Engineering*. 2001. p. 267-274.

40. De Gennes, P.G., et al., *Mechanoelectric effects in ionic gels.* Europhysics Letters, 2000. **50**(4): p. 513-518.

41. Bonomo, C., et al., *A method to characterize the deformation of an IPMC sensing membrane.* Sensors and Actuators, A: Physical, 2005. **A123-A124**: p. 146-154.

42. Farinholt, K.M. and D.J. Leo, *Effects of counter-ion, solvent type, and loading condition on the material response of ionic polymer transducers*, in *Proceedings of SPIE-The International Society for Optical Engineering*. 2004. p. 1-11.

43. Farinholt, K.M. and D.J. Leo, *Counterion and diluent effects on the response of ionic polymer transducers.* Journal of Intelligent Material Systems and Structures, 2007. **18**(7): p. 677-692.

44. Punning, A., M. Kruusmaa, and A. Aabloo, *Surface resistance experiments with IPMC sensors and actuators.* Sensors and Actuators A: Physical, 2007. **133**(1): p. 200-209.

45. Takagi, K., et al. *Frequency response characteristics of IPMC sensors with current/voltage measurements*. 2008: SPIE.

46. Shahinpoor, M., et al., *Ionic polymer-metal composites (IPMCs) as biomimetic sensors, actuators and artificial muscles. A review.* Smart Materials and Structures, 1998. **7**(6): p. R15-R30.

47. Ferrara, L., et al., *Use of ionic polymer-metal composites (IPMCs) as a pressure transducer in the human spine*, in *Proceedings of SPIE-The International Society for Optical Engineering*. 1999. p. 394-401.

48. Keshavarzi, A., et al., *Blood pressure, pulse rate, and rhythm measurement using ionic polymer-metal composite sensors*, in *Proceedings of SPIE-The International Society for Optical Engineering*. 1999. p. 369-376.

49. Tadokoro, S., et al. *An actuator model of ICPF for robotic applications on the basis of physicochemical hypotheses*. in *Robotics and Automation, 2000. Proceedings. ICRA '00. IEEE International Conference on*. 2000.

50. Etebari, A., et al., *A Dynamic Wall Shear Stress Sensor Based on Ionic Polymers*, in *ASME Fluids Engineering Division Summer Meeting*. 2005: Houston, TX.

51. Biddiss, E. and T. Chau, *Electroactive polymeric sensors in hand prostheses: bending response of an ionic polymer metal composite.* Medical Engineering and Physics, 2006. **28**(6): p. 568-78.

52. Punning, A., M. Kruusmaa, and A. Aabloo, *A self-sensing ion conducting polymer metal composite (IPMC) actuator.* Sensors and Actuators, A: Physical, 2007. **A136**(2): p. 656-664.

53. Wang, J., et al., *Design and fabrication of tactile sensors based on electroactive polymer composites*, in *Proceedings of SPIE-The International Society for Optical Engineering*. 2007, SPIE: San Diego, California, USA. p. 65241K-8.

54. Andò, B., et al., *A bio-inspired device to detect equilibrium variations using IPMCs and ferrofluids.* Sensors and Actuators A: Physical, 2008. **144**(2): p. 242-250.

55. Akle, B.J., et al., *Direct assembly process: a novel fabrication technique for large strain ionic polymer transducers.* Journal of Materials Science, 2007. **42**(16): p. 7031-7041.

56. Bennett, M.D. and D.J. Leo, *Ionic liquids as stable solvents for ionic polymer transducers.* Sensors and Actuators, A: Physical, 2004. **A115**(1): p. 79-90.

57. Andrew, J.D., et al. *Optimization of active electrodes for novel ionomer-based ionic polymer transducers*. 2008: SPIE.

58. Jeans, J.H., *Theoretical Mechanics*. 1907, Boston: Ginn and Company.

59. Abdulla, R., *The History of the Stethoscope.* Pediatric Cardiology, 2001. **22**: p. 371-372.

60. Mangione, S. and L.Z. Nieman, *Cardiac auscultatory skills of internal medicine and family practice trainees. A comparison of diagnostic proficiency.* JAMA, 1997. **278**(9): p. 717-722.

61. Iversen, K., et al., *A randomized trial comparing electronic and conventional stethoscopes.* The American Joural of Medicine, 2005. **118**: p. 1289e1-1289e4.

62. Schwartz, R., et al., *Improved phonocardiogram system based on acoustic impedance matching.* American Journal of Physiology, 1980. **238**: p. 604-608.

63. Scanlon, M.V., *Acoustic Sensor Pad for Physiological Monitoring.* Proceedings -19th international conference IEEE/EMBS, 1997: p. 747-750.

64. Scanlon, M.V., *Acoustic Sensor for Health Status Monitoring.* Proceeding of IRIS Acoustic and Seismic Sensing, 1998. **2**: p. 205-222.

65. Padmanabhan, V. and J.L. Semmlow, *Accelerometer Type Cardiac Transducer for detection of low level heart sounds.* IEEE TRANSACTIONS ON BIOMEDICAL ENGINEERING, 1993. **40**(1): p. 21-28.

66. Wood, J.C. and D.T. Barry, *Time-Frequency analysis of the first heart sound*, in *Engineering in Medicine and Biology, IEEE*. 1995. p. 144-151.

67. Guyton and Hall, *Textbook of Medical Physiology*. Vol. 11e. 2007: Elsevier.

68. Tavel, M.E. (2006) *Cardiac Auscultation: A glorious past- but does it have a future?* 1250-1253